Stationary solutions for the nonlinear Schrödinger equation modeling three-dimensional spherical Bose-Einstein condensates in general potentials

Kristina Mallory[*]
Division of Applied Mathematics, Brown University, 182 George Street, Providence, Rhode Island 02912, USA

Robert A. Van Gorder[†]
Oxford Centre for Industrial and Applied Mathematics, Mathematical Institute, University of Oxford, Andrew Wiles Building, Radcliffe Observatory Quarter, Woodstock Road, Oxford OX2 6GG, United Kingdom

(Received 4 December 2014; revised manuscript received 9 March 2015; published 1 July 2015)

Stationary solutions for the cubic nonlinear Schrödinger equation modeling Bose-Einstein condensates (BECs) confined in three spatial dimensions by general forms of a potential are studied through a perturbation method and also numerically. Note that we study both repulsive and attractive BECs under similar frameworks in order to deduce the effects of the potentials in each case. After outlining the general framework, solutions for a collection of specific confining potentials of physical relevance to experiments on BECs are provided in order to demonstrate the approach. We make several observations regarding the influence of the particular potentials on the behavior of the BECs in these cases, comparing and contrasting the qualitative behavior of the attractive and repulsive BECs for potentials of various strengths and forms. Finally, we consider the nonperturbative where the potential or the amplitude of the solutions is large, obtaining various qualitative results. When the kinetic energy term is small (relative to the nonlinearity and the confining potential), we recover the expected Thomas-Fermi approximation for the stationary solutions. Naturally, this also occurs in the large mass limit. Through all of these results, we are able to understand the qualitative behavior of spherical three-dimensional BECs in weak, intermediate, or strong confining potentials.

DOI: 10.1103/PhysRevE.92.013201 PACS number(s): 05.45.Yv, 04.25.Nx, 05.30.Jp

I. INTRODUCTION

We study stationary solutions to the cubic form of the nonlinear Schrödinger (NLS) equation modeling both repulsive and attractive Bose-Einstein condensates (BECs) in three spatial dimensions under radial traps. Note that the cubic NLS equation with potential has been used to model a dilute-gas BEC in the quasi-one-dimensional regime [1]. The scalar potential in the NLS equation can be used to model a confining potential or trap when dealing with applications to BECs. A variety of spatial traps have been utilized in the literature, and the specific application will often dictate the form of the trap employed [2]. Exact NLS equation solutions have been reported for a variety of potentials, and these include the Kronig-Penney potential [3] and the Jacobi sn potential [4] (in the case of the $1+1$ model). Single and multiwell potentials are possible, and in the latter case the use of appropriate multiwell potentials allows for a reasonable model of a dilute-gas BEC trapped in a standing light wave. In turn, BECs trapped in a standing light wave have been used to study phase coherence [5], matter-wave diffraction [6], quantum logic [7], and matter-wave transport [8]. Stationary solutions to the one-dimensional NLS equation under box and periodic boundary conditions were considered analytically for the repulsive [9] and attractive [10] cases, while BECs in a ring-shaped trap with a nonlinear double-well potential have also been considered [11]. PT-symmetric BEC solutions in a δ-function double-well potential have been studied [12]. Multiwell potentials make useful BEC traps in a number of physical scenarios [13].

A variety of potentials are used in the literature to study BECs, so in order to discuss these BEC solutions in sufficient generality, we should account for fairly general potential forms in our analysis. We consider a perturbation analysis of the solutions given small confining potentials that may take arbitrary forms. We perturbatively construct stationary solution states for the resulting equation under these arbitrary small potentials. In our analysis, we also consider radially symmetric traps and radially symmetric solutions to the resulting $3+1$ NLS equation. Physically, this assumption of radial symmetry is supported by a number of studies. Radial potentials (or potentials with nearly radial symmetry) or radial traps have been used to study BECs immersed in a Fermi sea [14], BECs in a dilute atomic vapor [15], BECs confined by dc electromagnets [16], vortex lattices in BECs [17], and rotating vortex lattices in BECs [18]. Indeed, such potentials are often useful when studying rotating BECs [19]. Radial potentials have also been used for other applications, such as the study of BEC collapse [20] and a sonic analog of gravitational black holes in BECs [21]. In three dimensions, this radial symmetry means that the potentials will exhibit spherical symmetry. Our analysis here extends our results for one-dimensional (1D) [22,23] and 2D [24] BECs under general potentials. However, owing to the fact that we now consider three spatial dimensions, there will be some differences between the present analysis and that which we have considered in previous work.

Since we assume radial symmetry of the stationary solutions, the cubic NLS equation reduces into a single nonlinear ordinary differential equation. In one spatial dimension, exact dark and bright soliton solutions can be found in closed form. However, in 3D, the ordinary differential equation involves a

[*]Corresponding author: kristina_mallory@brown.edu
[†]Robert.VanGorder@maths.ox.ac.uk

term $\frac{2}{r}\frac{d\Psi}{dr}$. This additional first derivative in the radial variable precludes the construction of a first integral, which complicates the solution procedure, so such closed-form solutions cannot be found. This is true of the 2D problem as well [24], and in that case the perturbation solutions can be expressed in terms of Bessel functions. For the 3D case, the solution representation will differ, as we demonstrate later. One can certainly argue the physical utility of studying 1D and 2D BECs for certain applications, but the relevance of 3D BECs is clear. While 1D BECs are often studied using traps with specific cylindrical symmetry (with the BEC tightly confined to the center of the cylinder), and 2D BECs will correspond to flat or surface traps (giving pancakelike structures), general 3D BECs are perhaps most relevant to a wider variety of experimental observations as they do not require such specific configurations. The types of 3D BECs we study here are assumed to have spherical radial symmetry, due to radially symmetric potentials chosen. Therefore, these BECs tend to aggregate into a spherical ball at the origin, with additional smaller density maxima occurring away from the origin in the form of shells around this central region. These BECs are amenable to mathematical and numerical analysis due, of course, to their radial symmetry.

In Sec. II we consider properties of stationary solutions in three spatial dimensions. In Sec. III, we construct perturbation solutions in the case of repulsive BECs under general potential functions, while we provide solutions for specific confining potentials in Sec. IV. Corresponding results are given for the attractive BECs in Secs. V and VI. We then obtain qualitative results for the nonperturbative regime in Sec. VII. Included are cases where the potential or the amplitude of the wave function is large. In the limit where the kinetic energy term is small relative to the size of the amplitude and the potential, we recover the Thomas-Fermi approximation. We also consider the very large mass limit. A discussion and some concluding remarks are given in Sec. VIII. From these various results, we gain a qualitative understanding of the influence of weak, intermediate, and strong potentials on the behavior and structure of 3D spherical BECs. These qualitative results are reinforced via a number of specific examples in which we consider specific physically relevant potentials from the literature.

II. STATIONARY SOLUTION

Let $V(\mathbf{x})$ be a scalar potential function. Then the $N+1$ cubic NLS equation (also referred to as the Gross-Pitaevskii model in some literature [25]) with small potential reads

$$i\hbar\Psi_t = \left[-\frac{\hbar^2}{2m}\nabla^2 + \epsilon V(\mathbf{x}) + g|\Psi|^2\right]\Psi, \tag{1}$$

where ϵ is a parameter which scales the potential function. For those unfamiliar with the notation $N+1$, we remark that the N denotes the spatial dimension, while the $+1$ signifies the time dimension. When $g>0$, we have the repulsive case, while when $g<0$ we have the attractive case. General perturbation results (of the type we seek here) were recently given for the $1+1$ model in Ref. [22] for the repulsive case and in Ref. [23] for the attractive case. In one spatial dimension, the repulsive case holds dark solitons as a special solution. Similarly, the attractive $1+1$ model will have bright solitons as a special class of solutions [23]. In Ref. [24], solutions in the particular case of two spatial dimensions were discussed via a form of perturbation. In the present paper, we are interested in expanding this work to the full physical case of three dimensions under radial potentials. Therefore, we henceforth take $V(\mathbf{x}) = V(r)$, where $r = \sqrt{x_1^2+x_2^2+x_3^2}$ denotes the radial coordinate.

We assume the general stationary state

$$\Psi(\mathbf{x},t) = \frac{\sqrt{2}\hbar}{\sqrt{m|g|}}\exp\left[-\mathrm{sgn}(g)\frac{\hbar}{2m}it\right]\psi(\mathbf{x}), \tag{2}$$

where ψ is a real-valued function. Then (1) is reduced to

$$\nabla^2\psi = -\mathrm{sgn}(g)\psi + \epsilon U(r)\psi + 2\mathrm{sgn}(g)\psi^3, \tag{3}$$

where

$$U(r) = \frac{2m}{\hbar^2}V(r). \tag{4}$$

Assuming that ψ is radial and small, in particular, of the form $\psi(\mathbf{x}) = \sqrt{\epsilon}\phi(r)$, the equation describing the behavior of ϕ is given by

$$\phi'' + \frac{2}{r}\phi' = -\mathrm{sgn}(g)\phi + \epsilon[U(r) + 2\mathrm{sgn}(g)\phi^2]\phi. \tag{5}$$

For a given form of $U(r)$, we are able to solve (5) in order to determine the behavior of the BEC wave function confined by that choice of potential $U(r)$.

III. PERTURBATION SOLUTIONS FOR GENERAL POTENTIALS IN REPULSIVE BECs

We begin by examining repulsive BECs. In order to construct perturbation solutions to (5) in this case, let us assume an expansion of the form

$$\phi(r) = \phi_0(r) + \epsilon\phi_1(r) + \epsilon^2\phi_2(r) + \cdots. \tag{6}$$

Under such an expansion, the stationary solution will read

$$\begin{aligned}\Psi(\mathbf{x},t) &= \Psi_0(\mathbf{x},t) + \epsilon\Psi_1(\mathbf{x},t) + \epsilon^2\Psi_2(\mathbf{x},t) + \cdots \\ &= \frac{\sqrt{2\epsilon}\hbar}{\sqrt{mg}}e^{-i\frac{\hbar}{2m}t}[\phi_0(r) + \epsilon\phi_1(r) + \epsilon^2\phi_2(r) + \cdots].\end{aligned} \tag{7}$$

Proceeding via the method, we determine the order-zero equation to be

$$\phi_0'' + \frac{2}{r}\phi_0' + \phi_0 = 0, \tag{8}$$

with conditions $\phi_0(0) = 1$ and $\phi_0'(0) = 0$. Thus, the order-zero term $\phi_0(r)$ takes the form

$$\phi_0(r) = \frac{\sin(r)}{r}. \tag{9}$$

Next, the order-one correction term will satisfy

$$\phi_1'' + \frac{2}{r}\phi_1' + \phi_1 = \left[2\phi_0^2 + U(r)\right]\phi_0, \tag{10}$$

along with the conditions $\phi_1(0) = 0$ and $\phi_1'(0) = 0$. Hence, the equation for ϕ_1 reads

$$\phi_1'' + \frac{2}{r}\phi_1' + \phi_1 = \left[\frac{2\sin^2(r)}{r^2} + U(r)\right]\frac{\sin(r)}{r}, \tag{11}$$

and ϕ_1 is given by

$$\phi_1(r) = \frac{1}{r}\int_0^r \frac{\sin(s)}{s^2}[2\sin^2(s) + U(s)s^2]W_1(r,s)ds, \quad (12)$$

where we have defined the function

$$W_1(r,s) = \sin(r)\cos(s) - \sin(s)\cos(r) = \sin(r-s).$$

Repeating the process for the order-two iteration, we may use ϕ_0, given in Eq. (9), to write the equation for ϕ_2 as

$$\phi_2'' + \frac{2}{r}\phi_2' + \phi_2 = \left[6\frac{\sin^2(r)}{r^2} + U(r)\right]\phi_1(r), \quad (13)$$

subject to $\phi_2(0) = 0$ and $\phi_2'(0) = 0$. Therefore, the order-two solution $\phi_2(r)$ reads

$$\phi_2(r) = \frac{1}{r}\int_0^r \frac{\phi_1(s)}{s}[6\sin^2(s) + U(s)s^2]W_1(r,s)ds. \quad (14)$$

IV. SOLUTIONS FOR REPULSIVE BECs IN SPECIFIC POTENTIALS

We have obtained a second-order perturbation theory for repulsive BECs in 3D given a general potential. Now we turn to many explicit examples of the potential in order to demonstrate our solution approach. Each of the potentials considered here is selected due to physical relevance, and for each we include pertinent citations demonstrating this relevance.

A. Constant potential

We consider first the case of a constant potential, that is, $U(r) = \lambda$, where $\lambda \in \mathbb{R}$. Note that the full repulsive equation in Eq. (5) cannot be solved exactly even when the potential is constant. This is different from the case of one spatial dimension, where the model is exactly solvable and a closed-form solution can be found. Consulting our perturbation approximation when U takes the functional form $U(r) = \lambda$, the zeroth-order term ϕ_0 remains as in Eq. (9) and the first-order term ϕ_1 will be

$$\phi_1(r) = \frac{1}{r}\int_0^r \frac{\sin(s)}{s^2}[2\sin^2(s) + \lambda s^2]W_1(r,s)ds. \quad (15)$$

Note that if we rewrite ϕ_1 as two integrals, viz.,

$$\phi_1(r) = \frac{2}{r}\int_0^r \frac{\sin^3(s)}{s^2}W_1(r,s)ds + \frac{\lambda}{r}\int_0^r \sin(s)W_1(r,s)ds, \quad (16)$$

we can quickly solve the second integral and determine that ϕ_1 takes the form

$$\phi_1(r) = \frac{2}{r}\int_0^r \frac{\sin^3(s)}{s^2}W_1(r,s)ds + \frac{\lambda}{2r}[\sin(r) - r\cos(r)]. \quad (17)$$

Moreover, the first integral, though complicated, can be written in closed form by way of special functions. To show this, let us call the former integral in Eq. (16) $I_1(r)$, that is,

$$I_1(r) = \frac{2}{r}\int_0^r \frac{\sin^3(s)\sin(r-s)}{s^2}ds. \quad (18)$$

Recalling the trigonometric identity

$$\sin^3(s)\sin(r-s) = \tfrac{1}{8}[\cos(r+2s) - \cos(r-4s)] + \tfrac{3}{8}[\cos(r-2s) - \cos(r)], \quad (19)$$

we observe that $I_1(r)$ takes the form

$$I_1(r) = \frac{1}{4r}\int_0^r \frac{\cos(r+2s) - \cos(r-4s)}{s^2} + \frac{3\cos(r-2s) - 3\cos(r)}{s^2}ds, \quad (20)$$

which is the integral we wish to evaluate. Let $J_1(r,s)$ be the antiderivative of

$$\frac{\cos(r+2s) - \cos(r-4s) + 3\cos(r-2s) - 3\cos(r)}{s^2}$$

in variable $s \geqslant 0$. Then we are concerned with determining both the upper limit $\lim_{s\to r} J_1(r,s)$ and the lower limit $\lim_{s\to 0^+} J_1(r,s)$. The first limit is not too complicated:

$$\lim_{s\to r} J_1(r,s) = J_1(r,r) = 4[\mathrm{Si}(4r) - 2\,\mathrm{Si}(2r)]\cos(r) + 4[\mathrm{Ci}(2r) - \mathrm{Ci}(4r)]\sin(r), \quad (21)$$

where

$$\mathrm{Si}(q) = \int_0^q \frac{\sin(t)}{t}dt,$$

$$\mathrm{Ci}(q) = \gamma + \ln q + \int_0^q \frac{\cos(t) - 1}{t}dt,$$

and $\gamma = 0.5772\ldots$ is the common Euler-Mascheroni constant. The lower limit $\lim_{s\to 0^+} J_1(r,s)$, however, is more challenging. We proceed by expanding $J_1(r,s)$ in a Taylor series about $s = 0$ (which is possible because r is real), to wit

$$J_1(r,s) = -4\ln(2)\sin(r) + \mathrm{O}(s^2). \quad (22)$$

Clearly, then,

$$\lim_{s\to 0^+} J_1(r,s) = -4\ln(2)\sin(r).$$

As such, $J_1(r,0)$ is well-defined (recall $s \geqslant 0$) and, in particular, $J_1(r,0) = -4\ln(2)\sin(r)$. Hence, we observe that

$$I_1(r) = \frac{J_1(r,r) - J_1(r,0)}{4r} = [\mathrm{Si}(4r) - 2\mathrm{Si}(2r)]\frac{\cos(r)}{r} + [\mathrm{Ci}(2r) - \mathrm{Ci}(4r) + \ln(2)]\frac{\sin(r)}{r}. \quad (23)$$

Since $I_1(r)$ is independent of the potential, it will appear in the order-one term of each of the following examples. Thus, we shall use $I_1(r)$ in place of the explicit expression (23) wherever it simplifies notation. Having calculated $I_1(r)$, we have that

$$\phi_1(r) = [\mathrm{Si}(4r) - 2\mathrm{S1}(2r)]\frac{\cos(r)}{r} - \lambda\cos(r) + \left[\mathrm{Ci}(2r) - \mathrm{Ci}(4r) + \ln(2) + \frac{\lambda}{2}\right]\sin(r). \quad (24)$$

In Fig. 1, we plot these solutions for a few values of λ and ϵ. In each case, the mass gathers in high concentration near

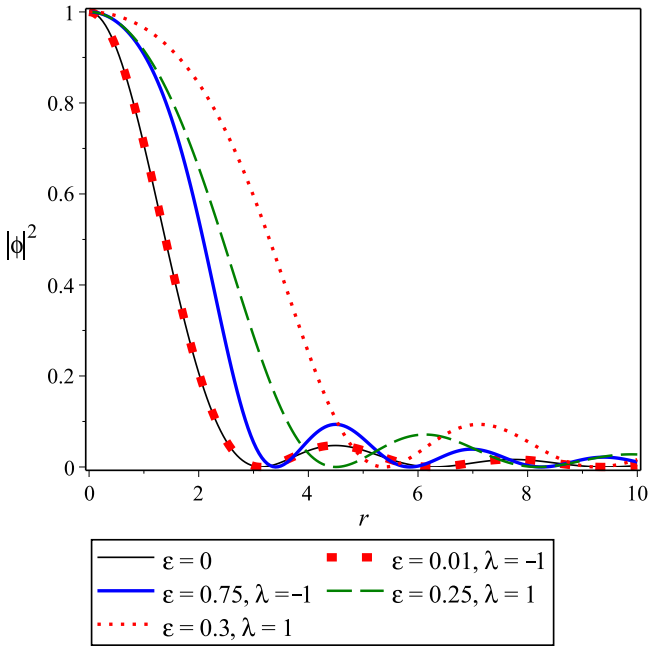

FIG. 1. (Color online) Density profiles for several repulsive solutions under the constant potential $U(r) = \lambda$.

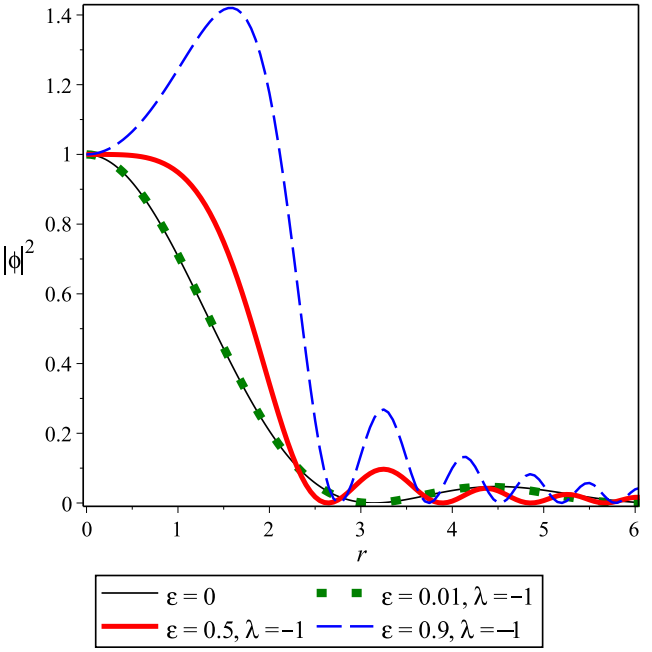

FIG. 2. (Color online) Density profiles for several repulsive solutions under the harmonic oscillator potential, which takes the form $U(r) = \lambda r^2$.

the origin. Remaining mass then gathers into smaller density maxima occurring at intermittent values of r, which gradually decay and vanish at finite r. We therefore find that the initial density peak is the primary one. Overall, the densities keep well with the unperturbed solution ϕ_0 when ϵ remains small. As ϵ becomes large, the rate of density decay decreases and the mass is kept less tightly to the origin, that is, the mass is able to reach larger r values. In general, we see that λ does not influence the structure of the density; however, solutions given a negative constant potential ($\lambda < 0$) agree more closely with the unperturbed case, even as ϵ grows.

Physically, the results correspond to scalings of the unconfined $3 + 1$ NLS equation solutions. In the repulsive case, the mass of the BEC is allocated in a central spherical region. Small density shells enclose this region, and the mass of these shells progressively decreases. However, unlike in the $1 + 1$ model, the secondary density maxima do not vanish. This is due to the fact that solitons are possible for the $1 + 1$ model, and hence all of the BEC mass can be allocated to a single wave envelope. Since there are no such solitons in the $3 + 1$ model, such a configuration is not possible unless the potential forces all of the mass of the BEC to be concentrated strongly in the center region. Hence, we see a number of cases in which these secondary density shells exist outside the primary region of mass centered at the origin.

B. Harmonic potential

Next let us examine repulsive BECs given a harmonic potential defined by $U(r) = \lambda r^2$ with $\lambda \in \mathbb{R}$. Harmonic potentials have been used as external potentials for BECs in a number of studies, as they serve as a relatively accurate and simple model of a parabolic trap [26]. It should be noted that such potentials can be generalized to include time dependence [27], but this is beyond the scope of the present paper, as such generalizations can deny us a stationary state of the kind we study here. One can construct a perturbation theory in this case by defining ϕ_0 as in Eq. (9) and taking the first-order solution (12) of the form

$$\phi_1(r) = \frac{1}{r}\int_0^r \frac{\sin(s)}{s^2}[2\sin^2(s) + \lambda s^4]W_1(r,s)ds. \tag{25}$$

As in the case of a constant potential, if we view ϕ_1 as

$$\phi_1(r) = I_1(r) + \frac{\lambda}{r}\int_0^r s^2 \sin(s) W_1(r,s)ds, \tag{26}$$

then the latter integral can be solved in closed form. In this way, ϕ_1 may be more simply represented by

$$\phi_1(r) = I_1(r) + \frac{\lambda}{12r}[(3r - 2r^3)\cos(r) + 3(r^2 - 1)\sin(r)]. \tag{27}$$

One can view the densities associated with these solutions for a few values of λ and ϵ in Fig. 2. For small ϵ, the density plots agree rather well with the unperturbed case. In those solutions having a negative potential (i.e., $\lambda < 0$), the mass clusters near the origin (into what we see as a large, initial peak) with a slight remainder gathering in subsequent, smaller peaks. At larger ϵ the rate of decay is more gradual and mass accumulates further across the radial domain. Nonetheless, we do not observe any mass spreading to very large r as the total mass always remains within some finite radial value. As we consider the large ϵ limit, solutions no longer agree with the unperturbed solution ϕ_0 on any interval and the density maximum occurs at some positive r value. Note that this difference occurs when ϵ no longer lies within the perturbative regime (where $\epsilon \ll 1$).

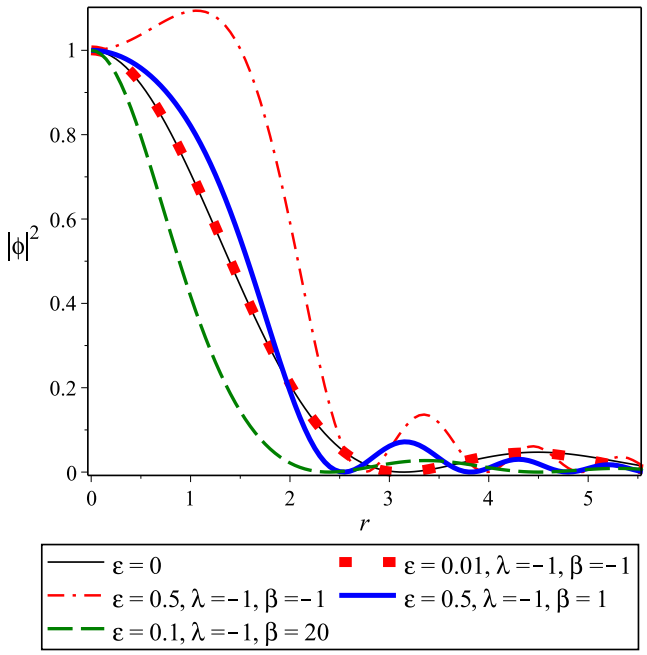

FIG. 3. (Color online) Density profiles for several repulsive solutions under the modified harmonic oscillator potential $U(r) = \lambda[r^2 + \beta \exp(-r^2)]$.

In the case where λ is positive, mass is no longer conserved (likely signifying unstable solutions) and solutions diverge even within the perturbative regime. Initially, however, the density plots follow the unperturbed case rather closely along the first density peak before diverging, suggesting that the mass is confined to the region very near $r = 0$.

Physically, we see that the small BECs ($\epsilon \ll 1$) are well confined by the harmonic trap. Most of their mass is confined to the center spherical region, with only relatively small density maxima occurring for larger values of the radial coordinate. On the other hand, when $\epsilon = O(1)$, the trap is not as effective, with relatively more of the mass of the BEC allocated in the secondary density shells.

C. Modified harmonic potential

Now let us consider the potential $U(r) = \lambda[r^2 + \beta \exp(-r^2)]$. There have been a number of modifications to the harmonic trap used in the literature [28], and one such potential is used here for sake of demonstration. The corresponding perturbation solution will take the form of that in Eqs. (9), (12), and (14). We omit the computational details here and examine the resultant densities $|\phi|^2$ in Fig. 3 given various λ, β, and ϵ. The structure we observe is quite regular in the context of potentials considered earlier. For solutions with $\lambda < 0$, the mass is mostly confined near the origin into a primary density peak. Subsequent, smaller peaks account for the remaining mass. As ϵ increases, we observe an expected trend: Solutions stray from the unperturbed case, allowing the mass to spread further radially. As seen in the case where $\epsilon = 0.5$ and $\lambda = -1$ are fixed, an increase in β from $\beta = -1$ to $\beta = 1$ results in the central mass density contracting toward the origin (as seen from comparing the red dashed line with the solid blue line). The increase from negative to positive β also decreases the amplitudes of the secondary density maxima. This makes sense, as an increase in β strengthens the confining potential. The green dashed line shows that for large positive β (here $\beta = 20$) the confining effects of the potential are amplified further, with the oscillating tail of the density plot smoothed.

On the other hand, when $\lambda > 0$, solutions behave like those under the harmonic oscillator potential. Plots diverge for all ϵ, likely due to unstable solutions, indicating that the mass is confined to the region very near $r = 0$.

The physics of the BECs under the modified harmonic trap is essentially the same as that under the harmonic trap. The small BECs ($\epsilon \ll 1$) are well confined by the modified harmonic trap, with only relatively small density maxima occurring outside the central region. Again, for larger ϵ, the secondary density shells contain a higher proportion of the BEC mass. We also notice that for small ϵ the change in BEC concentration with respect to radial variable is small, and the variation increases with increasing ϵ. This suggest that rapidly varying solution might be possible for large amplitude solutions. We explore this point in more detail in Sec. VII.

D. An asymmetric trap

The Morse potential is one example of an asymmetric trap [29,30] and is given by $U(r) = \lambda(e^{-2Ar} - 2e^{-Ar})$, where $\lambda > 0$ and $A > 0$ are typical parameters (although other signs can be considered). In contrast to the harmonic trap, the Morse potential increases more slowly along the positive r axis. In relation to BECs, the Morse potential has previously been considered for models of trapped atoms [31].

We consider the Morse potential, written $U(r) = \lambda(e^{-2Ar} - 2e^{-Ar})$. One may use the formulas in Sec. III to obtain the first-order perturbation solution corresponding to the Morse potential. We omit the details here and summarize the results in Fig. 4, which illustrates the density $|\phi|^2$ in some cases of λ, A, and ϵ. We observe that when $\lambda < 0$, much of the mass accumulates at $r = 0$, represented by a large peak near the origin, and a small remainder clusters into smaller, secondary peaks at intermediate radial values. In general, the mass spreads only up to some finite r value.

When $A < 0$, a rapid rate of decay signifies that mass is very strongly confined to those values near $r = 0$. As ϵ increases, this trap is strengthened. On the other hand, when $A > 0$, the mass spreads further across the radial domain. Contrary to the case where $A < 0$, an increase in ϵ actually weakens the trap, allowing a significant amount of mass to reach values away from $r = 0$.

In each case presented, we have considered a negative λ. When $\lambda > 0$, the solutions do not account for the conservation of mass as they become rapidly unbounded. This could signify that the density is confined to the region very near $r = 0$, as well as instability of the solutions.

We see that, for small ϵ, the Morse potential is rather effective at confining the BEC, with the secondary density maxima rapidly decaying in amplitude. So the BEC takes on a spherical from with only small amounts of mass present outside this core. For larger BEC [$\epsilon = O(1)$], the nonlinear effects become stronger, and the secondary density maxima

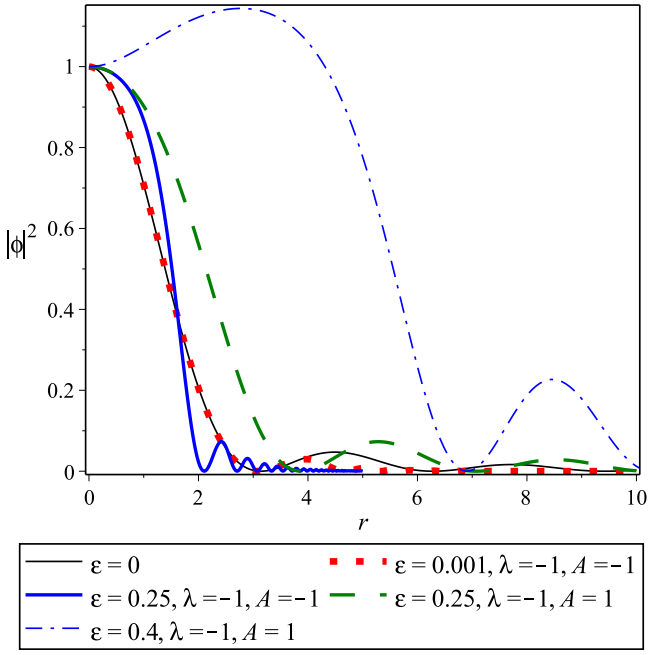

FIG. 4. (Color online) Density profiles for several repulsive solutions under the Morse potential $U(r) = \lambda(e^{-2Ar} - 2e^{-Ar})$.

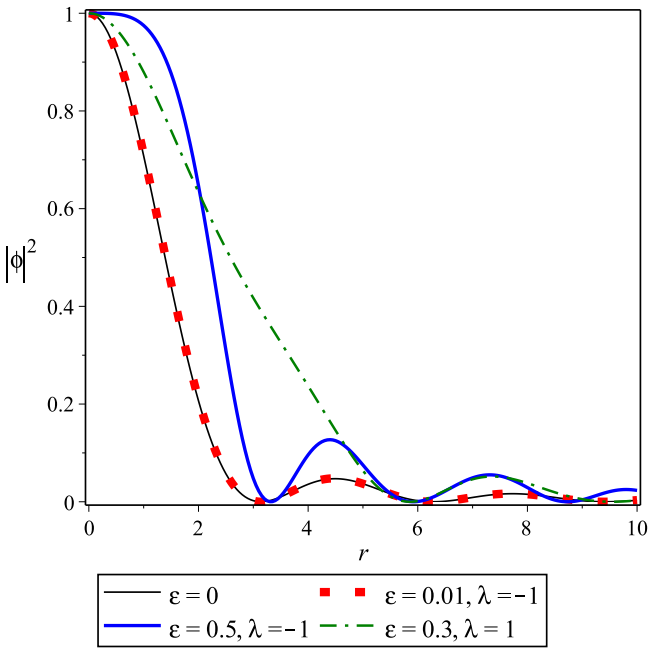

FIG. 5. (Color online) Repulsive solutions under the lattice potential $U(r) = \lambda[1 - \cos(r)]$.

hold more of the mass. Physically, the Morese potential appears most useful for confining small repulsive BECs.

E. Quantum pendulum potential: A lattice trap

The quantum pendulum potential takes the form $U(r) = \lambda[1 - \cos(r)]$. This is a good model of an optical lattice type potential, which has been used to study BECs in a number of settings [32]. The form we use here is that of a 3D radial lattice trap.

The perturbation solution (6) given the lattice trap potential may be constructed from the order-zero term (9) along with the order-one term (12) evaluated with $U(r) = \lambda[1 - \cos(r)]$, and so on. For clarity, ϕ_1 under this potential is more explicitly written

$$\phi_1(r) = I_1(r) + \frac{\lambda}{6r}[\sin(r) + \sin(2r) - 3r\cos(r)]. \quad (28)$$

Let us examine a few examples of these solutions in Fig. 5. Regardless of λ, the behavior of the density plots (for small enough ϵ) is rather regular in light of many of the previous examples. Here we see a significant accumulation of the mass near the origin into a primary density peak and a small remainder gathering via subsequent, secondary peaks which vanish at finite r. The value of ϵ influences the strength of the trap near the origin: As ϵ increases, the mass can spread further across the radial domain. Hence, smaller values of ϵ correspond to mass confined more tightly to the origin and closer agreement with the unperturbed case ϕ_0. Eventually, the potential weakening as ϵ grows allows the solutions to diverge at sufficiently large ϵ, which likely indicates that the mass becomes confined to the region very near $r = 0$. This expansion suggests that the solutions may be unstable.

The lattice potential gives somewhat interesting physical results. Although the trap is periodic with infinitely many wells, the mass of the BEC is still primarily contained within the central well, owing to the fact that the BEC is repulsive. For various values of the physical parameters, the secondary density maxima do occur in the outer potential wells. Therefore, the lattice trap can be useful for forcing the secondary density shells to occur at prescribed locations, which may be useful in experimental observations as this allows one to track the precise location of the secondary maxima. In contrast, for other types of potentials, the location of these maxima are due to the dynamics of the $3 + 1$ cubic NLS equation.

F. Double-well potential

Various applications call for double-well potentials [33]. One possible form of such a potential used is $U(r) = \lambda[(r^2 - 1)^2 - \beta]$, which gives a simple and symmetric double well. Given such a potential we can write the perturbation theory presented in Secs. III and IV by the zeroth-order solution (9) and the first-order solution (12), which now takes the form

$$\phi_1(r) = I_1(r) + \frac{\lambda}{60r}[(30\beta r - 105r + 50r^3 - 6r^5)\cos(r) + (105 - 30\beta - 75r^2 + 15r^4)\sin(r)]. \quad (29)$$

In Fig. 6 we plot these solutions for a few exemplary values of ϵ, λ, and β. The overall structure of the density when $\lambda < 0$ is not surprising; a large peak near the origin accounts for most of the mass, while smaller, subsequent peaks—vanishing at finite r—account for the rest. What is interesting here is the influence of β. We notice a clear dependence of the density on the value of β: As β increases, the trap at the origin weakens. Additionally, secondary peaks become taller so that more of the total mass occurs at intermediate r values. An increase in

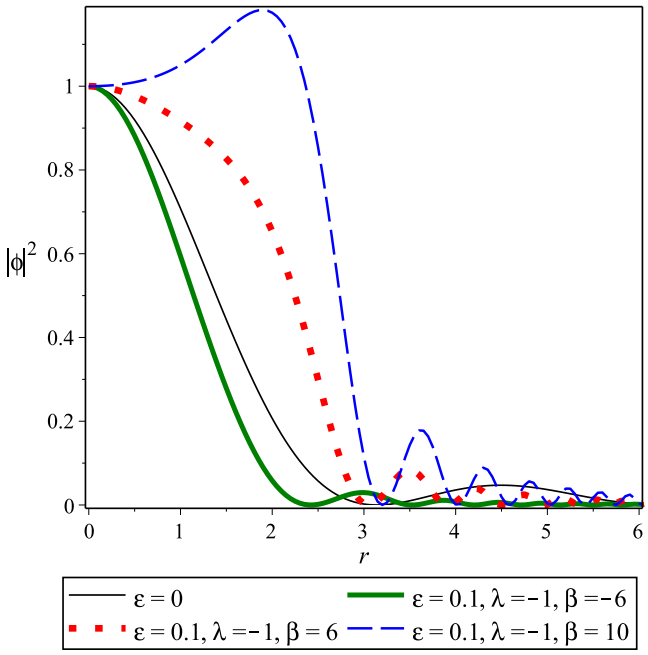

FIG. 6. (Color online) Density profiles for several repulsive solutions under the double-well potential $U(r) = \lambda[(r^2 - 1)^2 - \beta]$.

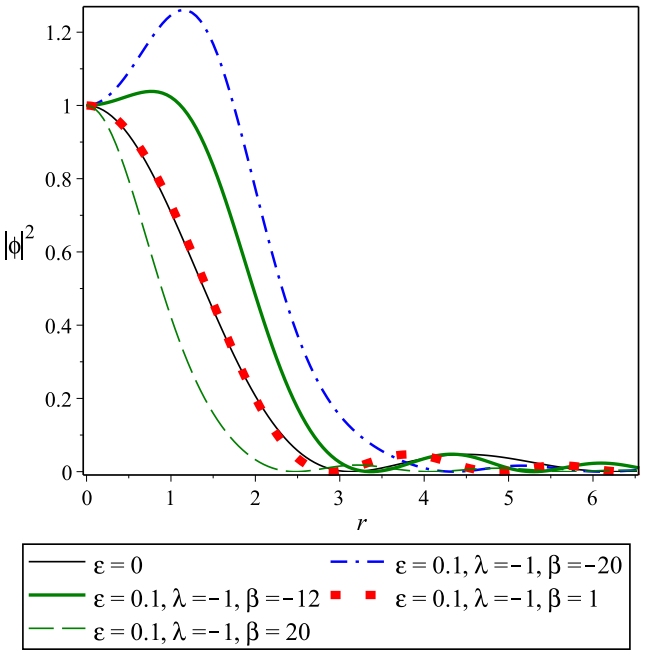

FIG. 7. (Color online) Density profiles for several repulsive solutions under the modified harmonic oscillator potential $U(r) = \lambda[r^2 + \beta \cos^2(r)]$.

β also places the density maximum away from the origin so that the mass is no longer in highest concentration at $r = 0$.

The density corresponding to solutions with positive λ exhibits rapid expansion, which increases as ϵ grows. This case is seemingly unstable (mass is not conserved) and suggests that mass is confined to the region very near the origin.

In physical terms, the double-well potential appears rather effective at confining much of the mass of the BEC to the core region near the origin. This makes sense in light of the fact that this potential is essentially a stronger form of the harmonic potential. While secondary density maxima do occur, they rapidly decay in amplitude as one moves radially away from the core region.

G. Harmonic potential with lattice trap

It is possible to combine a harmonic potential and lattice trap, or another collection of traps, to obtain pseudo- or quasiperiodic potentials; this type of potential has been considered previously in different settings [34]. One possible form of such a potential is $U(r) = \lambda[r^2 + \beta \cos^2(r)]$, which was used in Ref. [35]. This class of potential was shown to be useful for studying the 1D dynamics of a BEC of cold atoms in parabolic optical lattices [36]. Note that perturbation results can be obtained for a number of different types of lattice traps. We consider the potential $U(r) = \lambda[r^2 + \beta \cos^2(r)]$, since this potential is reasonably simple and has been considered elsewhere.

Under this assumption, the perturbation solution (6) will take ϕ_0 as in Eq. (9) and ϕ_1 as

$$\phi_1(r) = I_1(r) + \frac{\lambda}{24r}[3\beta \cos^2(r) \sin(r) + (6r + 3\beta r - 4r^3) \times \cos(r) + 6(r^2 - \beta - 1) \sin(r)]. \quad (30)$$

In Fig. 7, we plot the density $|\phi|^2$ for this perturbation solution given a potential of the form $U(r) = \lambda[r^2 + \beta \cos^2(r)]$. It is easy to observe the influence of β. While the mass appears to gather in a pattern similar to that under previous potentials, we find that a far smaller amount of the total mass lies outside of the initial density peak. In this case, then, nearly all of the mass clusters into a single peak near the origin. As β tends from negative to positive values, the strength of the confining potential increases and therefore we find more of the density allocated close to the origin. Furthermore, when the potential is weaker (for negative β), the maximal density is no longer located at the origin but at some positive value of the radius.

All of the plots examined take $\lambda < 0$. The $\lambda > 0$ case appears to be unstable as solutions become unbounded at finite r and, therefore, do not adhere to the conservation of mass. This density behavior indicates that mass is actually confined to the region very near $r = 0$.

Physically, the modified harmonic oscillator trap behaves much like the standard harmonic trap, with much of the mass of the BEC contained within the spherical core region and with the secondary density maxima decaying rapidly in amplitude. Despite the fact that there is a periodic term in the potential, the harmonic term dominates. This means that, unlike in the case of the lattice trap, the secondary density maxima do not occur at locations that are predictable only from the form of the potential.

V. PERTURBATION SOLUTIONS FOR GENERAL POTENTIALS IN ATTRACTIVE BECs

We now turn to the case of attractive BECs ($g < 0$) in 3D and proceed analogously to obtain the perturbation theory. Assuming an expansion of the form

$$\phi(r) = \phi_0(r) + \epsilon\phi_1(r) + \epsilon^2\phi_2(r) + \cdots, \quad (31)$$

the stationary solution will read

$$\Psi(\mathbf{x},t) = \Psi_0(\mathbf{x},t) + \epsilon\Psi_1(\mathbf{x},t) + \epsilon^2\Psi_2(\mathbf{x},t) + \cdots = \frac{\sqrt{2\epsilon}\hbar}{\sqrt{m|g|}} e^{i\frac{\hbar}{2m}t}[\phi_0(r) + \epsilon\phi_1(r) + \epsilon^2\phi_2(r) + \cdots]. \tag{32}$$

Under these assumptions, we determine the order-zero equation to be

$$\phi_0'' + \frac{2}{r}\phi_0' - \phi_0 = 0, \tag{33}$$

given the conditions $\phi_0(0) = 1$ and $\phi'(0) = 0$. Hence, the order-zero term $\phi_0(r)$ reads

$$\phi_0(r) = \frac{\sinh(r)}{r}. \tag{34}$$

Continuing with the higher-order terms, we find that the order-one solution ϕ_1 must satisfy

$$\phi_1'' + \frac{2}{r}\phi_1' - \phi_1 = [U(r) - 2\phi_0^2]\phi_0, \tag{35}$$

along with $\phi_1(0) = 0$ and $\phi_1'(0) = 0$. Since we can write the explicit form of the inhomogeneity with the aid of $\phi_0(r)$, this equation becomes

$$\phi_1'' + \frac{2}{r}\phi_1' - \phi_1 = \left[U(r) - \frac{2\sinh^2(r)}{r^2}\right]\frac{\sinh(r)}{r}, \tag{36}$$

and the first-order term $\phi_1(r)$ reads

$$\phi_1(r) = \frac{1}{r}\int_0^r \frac{\sinh(s)}{s^2}[s^2U(s) - 2\sinh^2(s)]W_2(r,s)ds, \tag{37}$$

where we define the function

$$W_2(r,s) = \sinh(r)\cosh(s) - \sinh(s)\cosh(r) = \sinh(r-s).$$

Next we see that $\phi_2(r)$ satisfies

$$\phi_2'' + \frac{2}{r}\phi_2' - \phi_2 = [U(r) - 6\phi_0(r)^2]\phi_1(r), \tag{38}$$

subject to $\phi_2(0) = 0$ and $\phi_2'(0) = 0$. Thus, imposing ϕ_0 in Eq. (34), the second-order solution $\phi_2(r)$ reads

$$\phi_2(r) = \frac{1}{r}\int_0^r \frac{\phi_1(s)}{s}[s^2U(s) - 6\sinh^2(s)]W_2(r,s)ds. \tag{39}$$

VI. SOLUTIONS FOR SPECIFIC POTENTIALS IN ATTRACTIVE BECs

Until now, we have obtained a second-order perturbation theory for attractive BECs with a general potential. To get a feel for the utility of these solutions, we illustrate their behavior by examining many explicit, relevant potentials as examples.

A. Constant potential

Let us begin by considering attractive BECs given the constant potential $U(r) = \lambda$, for $\lambda \in \mathbb{R}$. In this case, we obtain the perturbation theory taking $\phi_0(r)$ in Eq. (34) and $\phi_1(r)$ of the form

$$\phi_1(r) = \frac{1}{r}\int_0^r \frac{\sinh(s)}{s^2}[\lambda s^2 - 2\sinh^2(s)]W_2(r,s)ds, \tag{40}$$

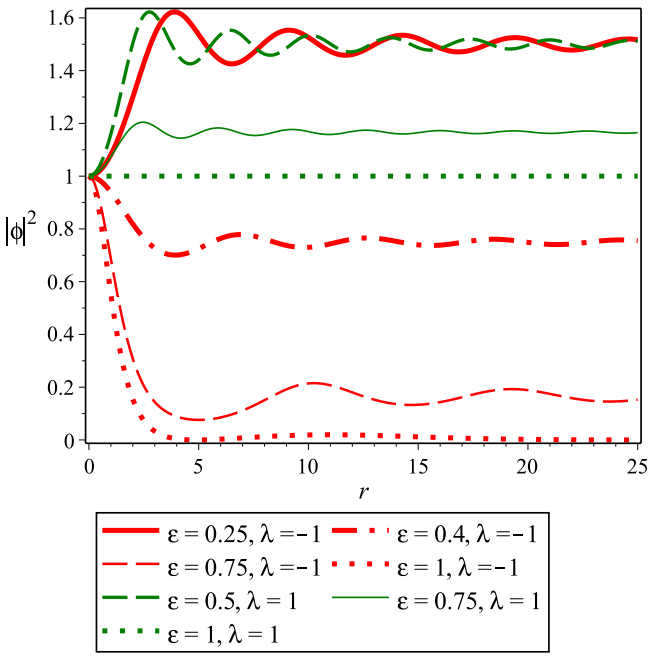

FIG. 8. (Color online) Density profiles for several attractive solutions under the constant potential $U(r) = \lambda$.

or, more simply,

$$\phi_1(r) = \frac{\lambda}{2r}[r\cosh(r) - \sinh(r)] - \frac{2}{r}\int_0^r \frac{\sinh^3(s)}{s^2}W_2(r,s)ds. \tag{41}$$

Let us define the integral term

$$I_2(r) = \frac{2}{r}\int_0^r \frac{\sinh^3(s)}{s^2}W_2(r,s)ds,$$

since it is independent of the potential and will appear in each of the subsequent examples. By an approach similar to that employed in Sec. IV A, we may write $I_2(r)$ in the form

$$I_2(r) = [\mathrm{Chi}(4r) - \mathrm{Chi}(2r) - \ln(2)]\frac{\sinh(r)}{r} + [2\mathrm{Shi}(2r) - \mathrm{Shi}(4r)]\frac{\cosh(r)}{r}, \tag{42}$$

where the functions $\mathrm{Chi}(r)$ and $\mathrm{Shi}(r)$ are defined as

$$\mathrm{Chi}(r) = \gamma + \ln(r) + \int_0^r \frac{\cosh(s) - 1}{s}ds, \tag{43}$$

$$\mathrm{Shi}(r) = \int_0^r \frac{\sinh(s)}{s}ds. \tag{44}$$

The function $\phi_1(r)$ can now be compactly written:

$$\phi_1(r) = \frac{\lambda}{2r}[r\cosh(r) - \sinh(r)] - I_2(r). \tag{45}$$

Figure 8 illustrates these solutions by plotting the density $|\phi|^2$ for a few choices of λ and ϵ. We see that, given a constant potential, the mass behaves differently in the attractive case than the repulsive case. Rather than remaining entirely near the origin, the mass now spreads across the r axis in nearly constant concentration. As ϵ increases, the quantity of mass at any positive r value decreases. Hence, the solutions existing

within the perturbative regime ($\epsilon \ll 0$) exhibit the largest concentration of mass at any given r.

We mention that the plots corresponding to attractive BECs do not include the density corresponding to the unperturbed solution $\phi_0(r) = r^{-1}\sinh(r)$. Contrary to the unperturbed solution in the repulsive case, the function $r^{-1}\sinh(r)$ diverges as $r \to +\infty$ rather quickly, which is true also for the density $|\phi_0|^2$, and such a density is unphysical. What this means is that the potential or the nonlinearity must be present in order for us to consider physically meaningful solutions; otherwise the density is not confined to a finite region and the solutions may expand.

Physically, the attractive BECs under constant potentials effectively are scaled versions of the radial stationary solutions to the attractive from of the $3+1$ cubic NLS equation. These solutions have a constant ambient density over space, and the density will slowly oscillate until this ambient value is attained. The physical parameters of the problem will determine exactly what this ambient concentration is, and we demonstrate how to calculate this value in the following section.

B. Asymptotic behavior as $r \to \infty$

In the previous example, we saw that a constant potential solution exists only for $\epsilon \neq 0$. Hence, there must be a potential present in order to permit a physically relevant solution. To see why, let us look at the asymptotic behavior of solutions with bounded potentials, that is, potentials which tend to some finite value as $r \to \infty$. In particular, we consider $U(r)$ such that $U(r) \to U_\infty$ as $r \to \infty$. Let us assume that the radial wave function tends to a finite value as $r \to \infty$, say $\phi(r) \to \phi^*$ in the limit $r \to \infty$. Then we have $\phi^* = \epsilon[\mathrm{sgn}(g)U_0 + 2\phi^{*2}]\phi^*$. We can show that, when $g > 0$ (the repulsive case), the solution $\phi^* = 0$ gives the stable equilibrium value. This agrees with the behavior exhibited in the density graphs given in Sec. IV. On the other hand, when $g < 0$ (the attractive case) we find that the stable equilibrium is given by

$$\phi^* = \sqrt{\frac{\epsilon^{-1} + U_\infty}{2}}. \tag{46}$$

Indeed, we observe a tendency for certain solutions to approach a positive equilibrium in the density plots of the present section. However, unlike with the repulsive case, this asymptotic behavior does not appropriately account for the $\epsilon \to 0$ limit. Unsurprisingly, in the attractive case we find that $\phi(r) \to \phi^* \sim \epsilon^{-1/2}$, and hence the $\epsilon \to 0$ limit constitutes a singular limit for the attractive case. This means that while the perturbation results for the small potential (the small ϵ case) in repulsive BECs are appropriate, we should numerically determine the solutions for the attractive case when ϵ is small, since the analytical solutions necessarily break down in the $\epsilon \to 0$ limit. As such, many results of this section are determined by numerically solving the second-order differential equation (5).

Again, these results are predicated on the existence of a limit $U(r) \to U_\infty$. If $U(r)$ does not approach a finite limit, then $\phi(r)$ may not approach the positive equilibrium value given in Eq. (46). Either $\phi(r)$ may not approach a finite limit, or $\phi(r)$ may approach the zero limit, depending on the specific form of the potential given. We see examples of each behavior as we explore various potential traps in this section.

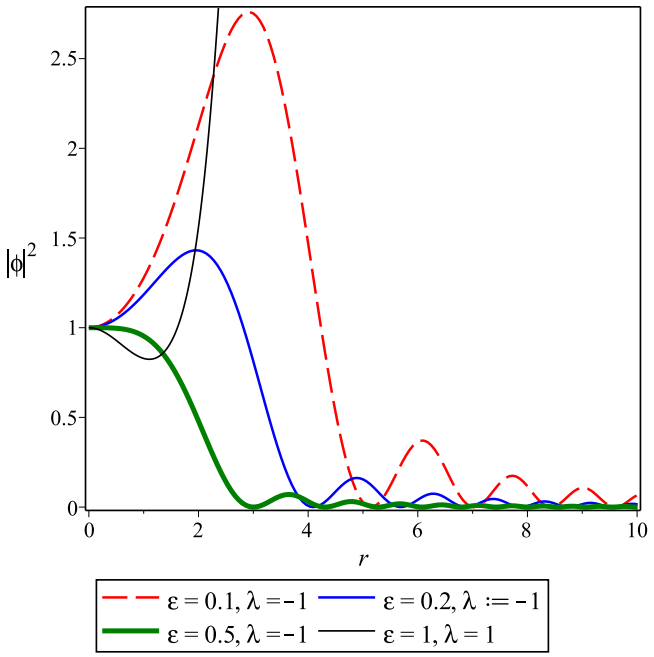

FIG. 9. (Color online) Density profiles for several attractive solutions under the harmonic oscillator potential, which takes the quadratic form $U(r) = \lambda r^2$.

C. Harmonic potential

Next we can consider attractive BECs given the harmonic oscillator potential $U(r) = \lambda r^2$ with $\lambda \in \mathbb{R}$. In this case, the perturbation solution constructed previously will take $\phi_0(r)$ in Eq. (34) and $\phi_1(r)$ of the form

$$\phi_1(r) = \frac{\lambda}{12r}[(2r^3 + 3r)\cosh(r) - (r^2 + 1)\sinh(r)] - I_2(r). \tag{47}$$

We explore these solutions under the harmonic oscillator potential $U(r) = \lambda r^2$ in Fig. 9. The density structure is rather regular when $\lambda < 0$. The mass is trapped near the origin, gathering into a large peak followed by a finite set of smaller, secondary peaks. With an increase in ϵ this trap is strengthened and a greater portion of the total mass clusters near the origin. This is precisely the opposite correspondence to that seen in solutions modeling repulsive BECs under the same potential. In that case, increasing ϵ causes the mass to distribute further across the domain and the maximum to exist further from the origin.

As was the case for repulsive BECs, solutions with $\lambda > 0$ are unbounded in finite r, indicating that the mass is confined to the area near $r = 0$. This expansion again suggests that the solutions may be unstable.

Physically, we see that the BECs confined by the harmonic trap are regular for $\lambda < 0$. In this case, the BECs are forced to have zero density for large values of the radial variable. In this case, the BEC mass is primarily confined to the core region, with secondary density shells decreasing in total mass as one moves radially out from the core region. This finding is true for both small and intermediate sized wave functions [$\epsilon \ll 1$ and $\epsilon = O(1)$].

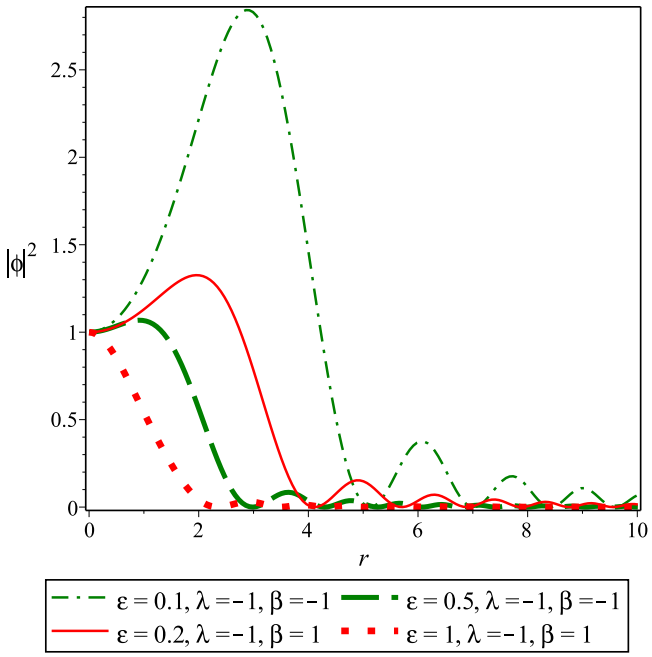

FIG. 10. (Color online) Density profiles for several attractive solutions under the modified harmonic oscillator potential $U(r) = \lambda[r^2 + \beta \exp(-r^2)]$.

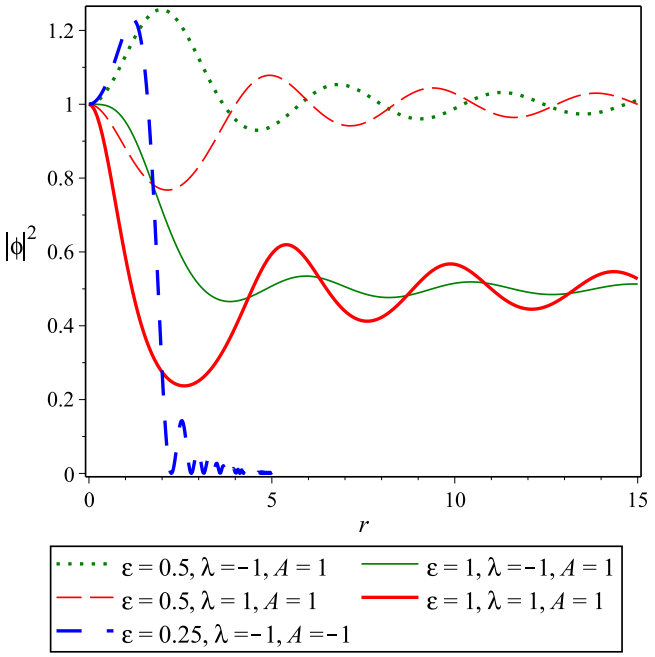

FIG. 11. (Color online) Density profiles for several attractive solutions under the Morse potential $U(r) = \lambda(e^{-2Ar} - 2e^{-Ar})$.

D. Modified harmonic potential

We consider solutions for the potential $U(r) = \lambda[r^2 + \beta \exp(-r^2)]$ and plot the densities in Fig. 10. When $\lambda < 0$, we observe a tendency for the mass to remain confined to the origin, gathering mostly into an initial density peak. Despite the sign of β, an increase in ϵ causes a stronger pull of the mass toward $r = 0$. Moreover, increasing ϵ translates the density maximum closer to the origin and results in more of the total mass contained within the primary peak. This effect certainly contrasts the behavior of solutions modeling repulsive BECs given the same potential (see Sec. V C). In that case, the value of β greatly influenced the strength of the trap at the origin.

Figure 10 avoids those solutions which have a positive λ as those plots grow rapidly without bound, of course, indicating that the solutions do not account for mass conservation. As in earlier sections, this suggests that the mass is likely confined very near the origin.

In the case of the modified harmonic trap, the physical reasoning is the same as for the standard harmonic trap. For an appropriately signed trap, regular solutions exist and these solutions are primarily confined to the spherical core region. The secondary density maxima decrease in total mass fairly rapidly as one moves radially away from the core region.

E. An asymmetric trap

We consider solutions under the Morse potential $U(r) = \lambda(e^{-2Ar} - 2e^{-Ar})$ and plot the densities in Fig. 11. The detail to note here is the influence of the parameter A. When $A < 0$, the density admits a global maximum very near the origin then decays rapidly to zero. This behavior signifies that nearly all of the mass is confined to the radial values near $r = 0$; smaller local density maxima account for the minimal remaining mass. This extreme rate of decay, confining nearly all of the mass to the area near $r = 0$, is common to both repulsive and attractive BECs with this potential.

The case in which A is positive differs greatly in structure. Contrary to the repulsive case, these densities actually oscillate about a positive value as r becomes large. Accordingly, the mass is not confined to the origin, but is able to disperse across the radial domain with a nearly constant concentration. Hence, when $A > 0$, which is typical, the mass behaves qualitatively differently depending on the repulsiveness or attractiveness of the BECs.

The Morse potential is an example of a physical trap that remains of bounded strength and hence is much weaker than, say, a harmonic trap. As a result, the solutions in many of the cases considered share the physical properties of unconfined attractive BECs. For the case where the potential is bounded ($A > 0$), the attractive BECs tend to their ambient positive values, and hence while there density oscillations, the whole region $r \geqslant 0$ acts as one density cloud. The exception is when we pick $A < 0$, for which the trap becomes unbounded in the radial coordinate. Such a trap is strong (much stronger even than the harmonic potential, due to the exponential rate of strengthening) and hence confines the mass of the BEC to a core region near the origin. Any secondary density maxima decreases in size rapidly as we move radially outward from this core region. Therefore, when $A < 0$, the trap is highly effective at containing the attractive BEC, while when $A > 0$, the trap simply modifies the small radius behavior of the BEC before they tend toward their natural asymptotic vales.

F. Quantum pendulum potential: A lattice trap

Figure 12 shows the densities under the quantum pendulum potential $U(r) = \lambda[1 - \cos(r)]$ for various values of the

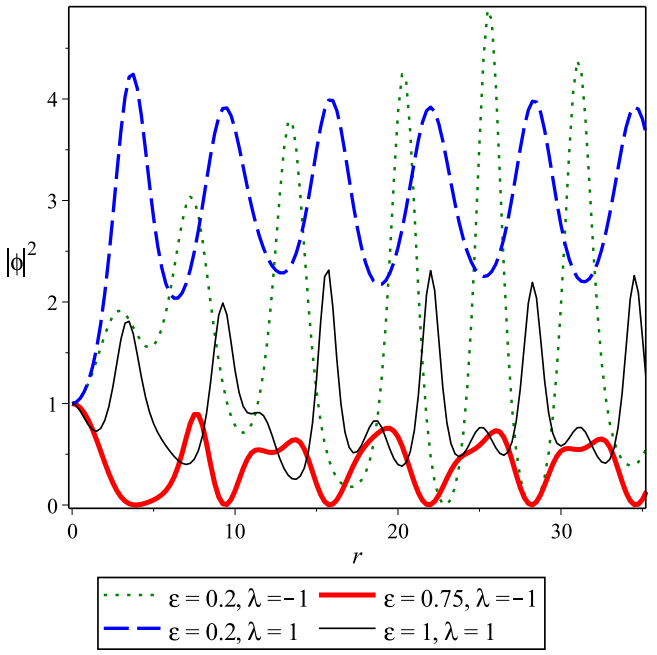

FIG. 12. (Color online) Density profiles for several attractive solutions under the lattice potential $U(r) = \lambda[1 - \cos(r)]$.

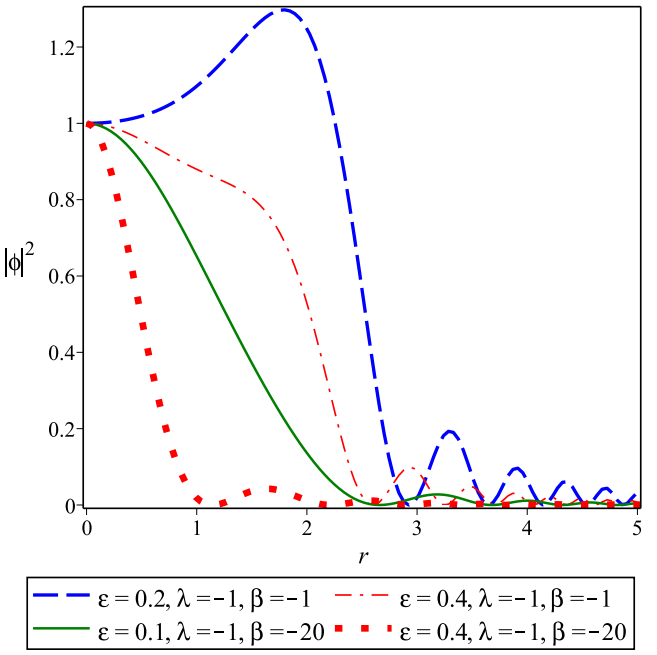

FIG. 13. (Color online) Density profiles for several attractive solutions under the double-well potential $U(r) = \lambda[(r^2 - 1)^2 - \beta]$.

parameters λ and ϵ. In this case, we observe a mass distribution qualitatively different from that seen when we study repulsive BECs. For all values of λ and ϵ, the mass is not confined to the area between the origin and some finite radius, but instead spreads throughout the problem domain. Not unlike previous cases, the mass gathers in large quantities at periodic radial values (represented by local density maxima which we can expect to continue across the r axis). However, what is unique in this case is the lack of density decay, accounting for the presence of a nontrivial portion of the mass at all r. This is not surprising given the influence of a cosine function in the potential; however, it does stand in stark contrast to the behavior of the repulsive case under the same potential.

Physically, the lattice trap refocuses the density oscillations in the BECs to align with the potential wells of the trap. For all parameter values taken, these BEC solutions have maximal density in the center of each potential well in the lattice potential. The density profiles do not tend to any constant asymptotic value. Rather, the behavior observed continues as one moves radially away from the origin. The physical picture is then of a succession of density shells, each occurring at radial distances corresponding to the potential wells in the lattice potential. This allows one to predict where to experimentally obtain the highest concentration of the BEC, implying the usefulness of such a confining trap.

G. Double-well potential

The double-well potential takes the form $U(r) = \lambda[(r^2 - 1)^2 - \beta]$. Given such a potential, we may construct the perturbation theory via ϕ_0 in Eq. (34) and ϕ_1 given by

$$\phi_1(r) = \frac{\lambda}{60r}[(6r^5 + 10r^3 + 45r - 30\beta r)\cosh(r) - 15(r^4 + r^2 - 2\beta + 3)\sinh(r)] - I_2(r). \quad (48)$$

In Fig. 13 we illustrate the densities for some choices of the parameters λ, β, and ϵ. We find that the mass behaves qualitatively similarly under the double-well potential whether the BECs are attractive or repulsive. When $\lambda < 0$, most of the mass accumulates at the origin via one primary density peak, while secondary peaks which gradually decay and vanish at finite r account for a small remainder. As β shrinks, the trap confining the mass to the origin strengthens. Thus, the value of β determines to what extent the mass can spread along the r axis.

The case where $\lambda > 0$ appears to be unstable and results in a density which becomes rapidly unbounded at small, finite r. Despite mathematically disregarding the conservation of mass, such a density suggests that the mass is confined to the region very near the origin.

As was noted for the repulsive BEC, the double-well potential is effective at confining the attractive BECs, as well. Physically, such a trap could be used to ensure that most of the mass of the BEC remains within a spherical core region, with only small amounts of mass allocated to the secondary density shells. Interestingly, the trap is effective even when $\epsilon = O(1)$ (i.e., when the wave functions are of intermediate amplitude). The additional parameter, β, can be used to tune the trap so that the desired concentration of BEC can be found in the core region. When $\beta \to 0$, the trap reduces to what is essentially a stronger version of the harmonic trap.

H. Harmonic potential with lattice trap

In Fig. 14, we plot the densities $|\phi|^2$ for solutions given a potential of the form $U(r) = \lambda[r^2 + \beta\cos^2(r)]$. We observe no qualitative differences between repulsive BECs and attractive BECs. As with many other potentials, the modified harmonic oscillator potential with negative λ works to confine the mass

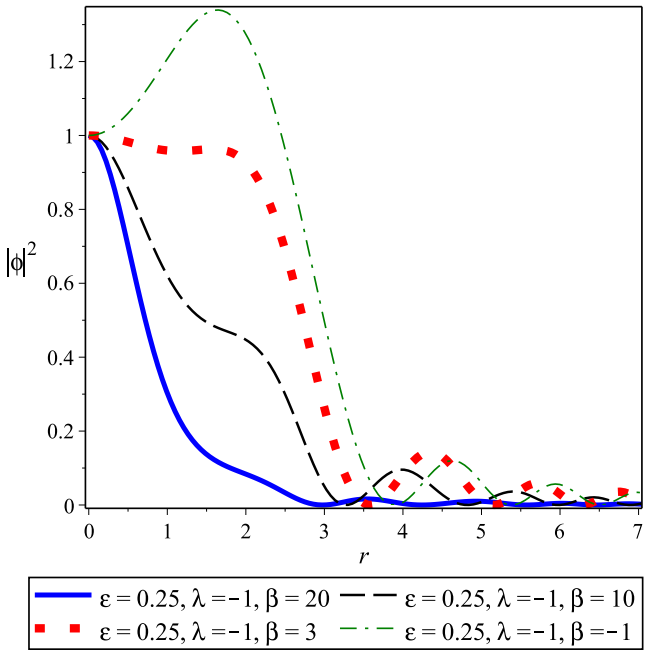

FIG. 14. (Color online) Density profiles for several attractive solutions under the modified harmonic oscillator potential $U(r) = \lambda[r^2 + \beta\cos^2(r)]$.

to the area near the origin. Specifically, the mass gathers in highest concentration via a large peak at the origin and then in lesser quantity within smaller, decaying peaks. These peaks vanish in finite r and hence mass is not present across the entire radial domain. The density maximum, however, does not always occur at $r = 0$. Instead, its location is dependent on the value of β: As β shrinks, the global maximum density (and highest concentration of mass) is shifted further from the origin. Such a translation results in a similar shift of the subsequent local maxima and, hence, smaller β also weakens the trap at the origin, allowing the mass to reach larger radial values.

On the other hand, the potential no longer traps the mass when $\lambda > 0$, and the plots quickly diverge (likely due to unstable solutions). This divergence suggests that the density is confined only to the region very near $r = 0$.

The composite harmonic trap with lattice term is also physically useful for ensuring that the attractive BEC is mostly confined to the core spherical region surrounding the origin. While the tuning parameter β influences the specific form of this core region, note that for all nonzero β values, we see that the trap is effective at forcing secondary density maxima to decay sufficiently rapidly.

VII. THE NONPERTURBATIVE REGIME

In the above, we have considered the perturbative case in which $\psi(\mathbf{x}) = \sqrt{\epsilon}\phi(r)$ analytically for small ϵ, while the potential was also taken as small near the origin. For a number of examples, we also gave numerical solutions in the case where $\epsilon = O(1)$. In this present section, we turn our attention toward qualitative results for the case in which one or both of the nonlinearity or the potential are not small relative to the kinetic energy term. In this case, we drop ϵ from (1)

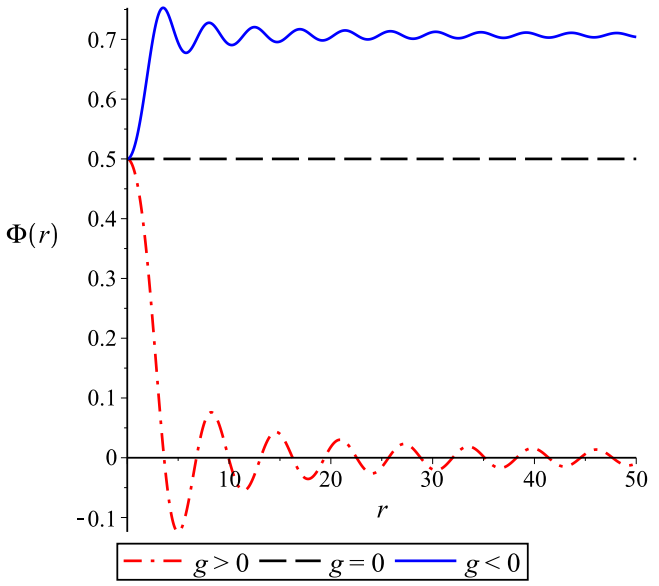

FIG. 15. (Color online) Plot of the wave function solutions to (53) when $\epsilon = 0$. This gives us the radial solutions to the $3+1$ cubic NLS equation. The results are in qualitative agreement with the density plots obtained in prior sections when both small amplitude wave functions and small potentials were considered. Initial conditions are taken to be $\Phi(0) = \Phi_0 = 0.5$ and $\Phi'(0) = 0$.

and have

$$i\hbar\Psi_t = \left[-\frac{\hbar^2}{2m}\nabla^2 + V(\mathbf{x}) + g|\Psi|^2\right]\Psi. \tag{49}$$

Assuming a radial solution of the form

$$\Psi(\mathbf{x},t) = \frac{\sqrt{2}\hbar}{\sqrt{m|g|}}\exp\left[-\mathrm{sgn}(g)\frac{\hbar}{2m}it\right]\Phi(r), \tag{50}$$

and writing the scaled potential as

$$\mathcal{U}(r) = \frac{2m}{\hbar^2}V(r), \tag{51}$$

we find that the stationary state $\Phi(r)$ is governed by the equation

$$\Phi'' + \frac{2}{r}\Phi' + \mathrm{sgn}(g)(\Phi - 2\Phi^3) = \mathcal{U}(r)\Phi. \tag{52}$$

The initial conditions will be of the form $\Phi(0) = \Phi_0$, $\Phi'(0) = 0$. If $\mathcal{U}(r) = \epsilon U(r)$, we recover the small-potential limit. If, additionally, $\Phi(r) = \sqrt{\epsilon}\phi(r)$, then we recover the perturbative case for small amplitude wave functions.

A. Small potential, intermediate amplitude limit

In the limit where the confining potential is small, but the wave function is not small, we should have

$$\Phi'' + \frac{2}{r}\Phi' + \mathrm{sgn}(g)(\Phi - 2\Phi^3) = \epsilon U(r)\Phi. \tag{53}$$

In this limit, the wave functions act simply as solutions to the $3+1$ cubic NLS equation under radial symmetry. In Fig. 15, we plot sample solutions for $g > 0$ (the repulsive case), $g = 0$ (the linear case), and $g < 0$ (the attractive case). The results are qualitatively similar to what we have observed in several of

the plots obtained in previous sections. In the attractive case, the solutions exhibit damped oscillations toward some positive asymptotic value. In the repulsive case, the radial part of the wave function exhibits damped oscillations as it decays to zero. The linear case is trivial, as the only solution in this case is the radially constant solution. Therefore, the oscillations in the density plots obtained in the perturbative limit are completely consistent with what one should expect from the solutions in which the full nonlinearity is maintained (when there is no perturbation due to a small amplitude).

Physically, we see that the unconfined solutions to the $3+1$ attractive cubic NLS equation give BECs which oscillate in density before tending toward an ambient density level. These BECs therefore exist in a type of spherical cloud that maintains the ambient density level as the radial variable becomes large. This is in contrast to, say, a soliton solution to the $1+1$ cubic NLS equation, in which all of the density is located within a (relatively) small wave envelope. For the repulsive case, we see that unconfined solutions to the $3+1$ repulsive cubic NLS equation result in BECs that have most of their density allocated to a spherical core region centered at the origin. There then exist secondary and much smaller density shells surrounding this core region. These density shells gradually decrease in mass as one moves radially away from the central core region. Note that these density fluctuations (or oscillating tails) are a fundamental part of the solution to radial cubic NLS equations in three spatial dimensions. They also appear in the 2D case. The 1D case is integrable and permits solitons, which do not exhibit such oscillations. However, distinct types of oscillating solutions can still be found for the 1D cubic NLS equation (such as solutions in terms of elliptic functions). Therefore, when selecting a potential, one must decide on whether the oscillating tails are permissible or not. If not, one should select a potential which will cause any such secondary density maxima to be as small as needed.

One can similarly solve (53) when $\epsilon > 0$ to obtain results for intermediate potentials and intermediate wave function amplitudes. These numerical plots are included alongside several of the density plots in previous sections and do not need to be reproduced here. However, in Fig. 16, we plot the solutions due to small lattice potentials. It is clear that such results are effectively perturbations of the solutions observed in Fig. 15. The exception is when $g = 0$ (the linear case), because in the presence of a potential this solution can no longer behave like a fixed point and hence the potential dominates. Note that in many cases there are quantitative changes in the solutions under the potentials, but the qualitative behavior of the wave functions is similar in both the small and the intermediate amplitude regimes in many cases.

Physically, this case corresponds to the very small mass limit, since $\mathcal{U} = O(m)$ for small mass m by Eq. (51). Hence, in the very small mass limit, the BECs behave like solutions of the free (unconfined) solution to the $3+1$ cubic NLS equation.

B. Large potential, large amplitude limit, and the Thomas-Fermi approximation

While we have considered solutions for small or intermediate potentials [$\epsilon \ll 1$ or $\epsilon = O(1)$], the large confining potential is useful to study. This case is physically relevant in the sense that a large or strong potential can be used to confine a small BEC. The Thomas-Fermi case corresponds then to the case where the radial potential $\mathcal{U}(r) \gg 1$. To this end, let ϵ remain a small parameter, and consider $\mathcal{U} = \epsilon^{-1}\overline{U}(r)$. It makes sense to consider a large amplitude radially symmetric stationary solution of the form $\Phi(r) = \epsilon^{-1/2}\overline{\Phi}(r)$, which yields the stationary ordinary differential equation

$$\overline{\Phi}'' + \frac{2}{r}\overline{\Phi}' + \mathrm{sgn}(g)\overline{\Phi} = \epsilon^{-1}[2\mathrm{sgn}(g)\overline{\Phi}^2 + \overline{U}(r)]\overline{\Phi}. \quad (54)$$

In the very small ϵ limit, we must have $2\mathrm{sgn}(g)\overline{\Phi}^2 + \overline{U}(r) \to 0$ as $\epsilon \to 0$. So, in the very large potential case, we must have the scaling

$$\overline{\Phi}(r) \sim \sqrt{-\frac{\mathrm{sgn}(g)}{2}\overline{U}(r)} \quad (55)$$

in the $\epsilon \to 0$ limit. In such a limit, the kinetic energy is negligible compared to the nonlinearity, and this is the Thomas-Fermi limit. Indeed, (55) is the Thomas-Fermi approximation for the $3+1$ model.

In the case where the potential is large (but not so large that $\epsilon \to 0$), we can still study the solutions. From the form of (54), it makes sense to consider a solution that varies rapidly over space. So let us consider

$$\overline{\Phi}(r) = \hat{\Phi}(R), \quad \overline{U}(r) = \hat{U}(R), \quad \text{where} \quad R = \frac{r}{\sqrt{\epsilon}}. \quad (56)$$

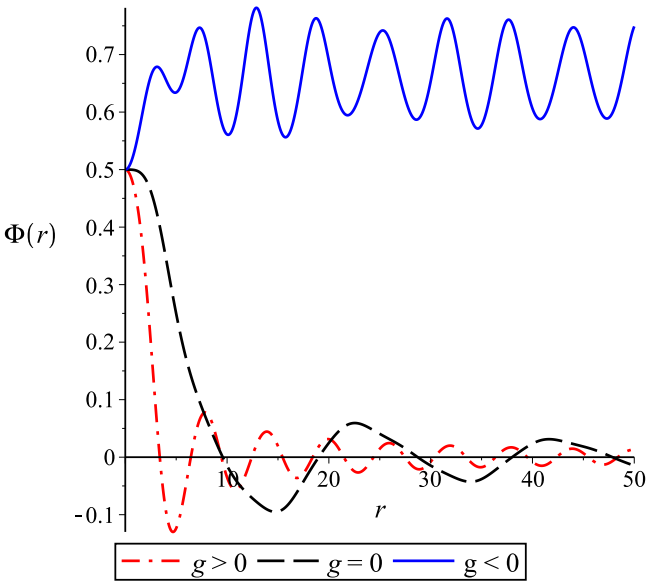

FIG. 16. (Color online) Plot of the wave function solutions to (53) when $\epsilon = 0.1$, $U(r) = -[1-\cos(r)]$. This gives us perturbations to the radial solutions to the $3+1$ cubic NLS equation due to the small potential. The results are in qualitative agreement with Fig. 15 for the attractive and repulsive solutions. The primary difference is that the oscillations in the radial part of the wave function are amplified, due to the form of the potential. For the linear case $g = 0$, the solution is drastically different, as we are no longer at a steady state. The linear case behaves qualitatively similarly to the repulsive case. Initial conditions are taken to be $\Phi(0) = \Phi_0 = 0.5$ and $\Phi'(0) = 0$.

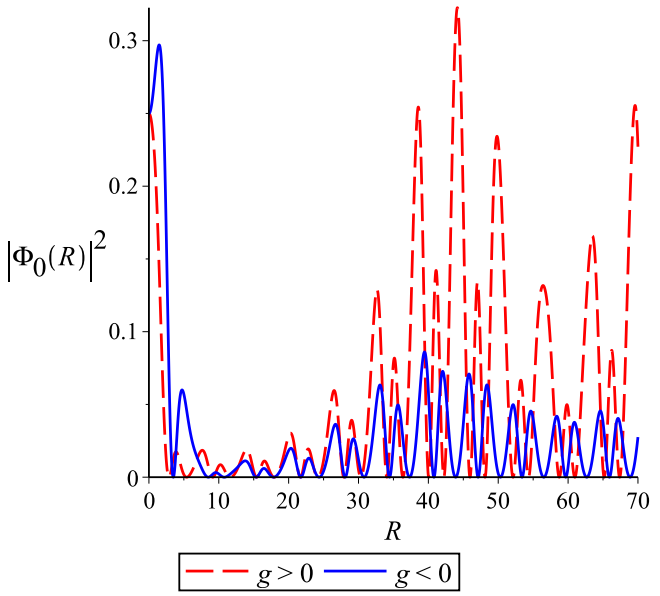

FIG. 17. (Color online) Plot of the scaled density for wave function solutions to (60) in the case of both repulsive ($g < 0$) and attractive ($g > 0$) BECs confined by the large lattice potential (61). Initial conditions are taken to be $\Phi_0(0) = 0.5$ and $\Phi_0'(0) = 0$. To recover the true density, one would multiply $|\Phi_0(R)|^2$ by a factor of ϵ^{-1} [since $\Phi(r) = O(\epsilon^{-1/2}$ in this case], which would give $|\Phi(r)|^2 = \epsilon^{-1}|\Phi_0(r/\sqrt{\epsilon})|^2$. The large potential has a stronger influence on the density of the BECs than does the nonlinearity.

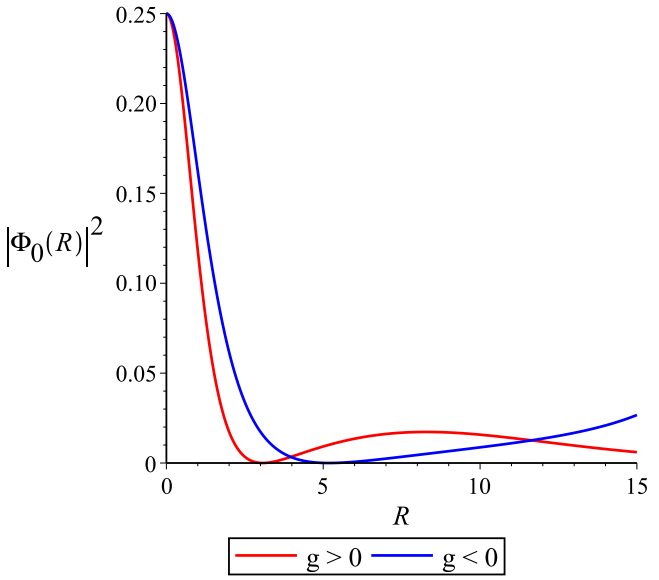

FIG. 18. (Color online) Plot of the scaled density for wave function solutions to (60) in the case of both repulsive ($g < 0$) and attractive ($g > 0$) BECs confined by the large Morse potential (62). Initial conditions are taken to be $\Phi_0(0) = 0.5$ and $\Phi_0'(0) = 0$. To recover the true density, one would multiply $|\Phi_0(R)|^2$ by a factor of ϵ^{-1} [since $\Phi(r) = O(\epsilon^{-1/2})$ in this case], which would give $|\Phi(r)|^2 = \epsilon^{-1}|\Phi_0(r/\sqrt{\epsilon})|^2$. We see that the large potential dominates the dynamics of both solutions, with only minor differences seen between the attractive and repulsive BECs. The large potential confines most of the mass to near the origin.

This puts (54) into the form

$$\hat{\Phi}'' + \frac{2}{R}\hat{\Phi}' - [2\mathrm{sgn}(g)\hat{\Phi}^2 + \hat{U}(R)]\hat{\Phi} = -\epsilon \mathrm{sgn}(g)\hat{\Phi}. \quad (57)$$

Clearly, we should seek a solution of the form

$$\hat{\Phi}(R) = \Phi_0(R) + \epsilon\Phi_1(R) + O(\epsilon^2). \quad (58)$$

In turn, this will give the stationary solution

$$\Phi(r) = \frac{1}{\sqrt{\epsilon}}\Phi_0\left(\frac{r}{\sqrt{\epsilon}}\right) + O(\sqrt{\epsilon}); \quad (59)$$

hence, for small ϵ the Φ_0 term will dominate and give the interesting qualitative features of the solution. As was the case in two spatial dimensions [24], the larger the amplitude becomes, the smaller the error term will be. For example, if the potential scales as 10^{2k} units, the amplitude scales as 10^k units while the correction scales as 10^{-k} units (a difference of $2k$ orders of magnitude between the amplitude and the error). From (57) we see that $\Phi_0(R)$ must satisfy the equation

$$\Phi_0'' + \frac{2}{R}\Phi_0' = 2\mathrm{sgn}(g)\Phi_0^3 + \hat{U}(R)\Phi_0. \quad (60)$$

Equation (60) is nonlinear and nonautonomous, so we seek numerical solutions.

In Fig. 17 we plot the density for both attractive and repulsive BECs for the lattice potential $\hat{U}(R) = \cos(R) - 1$, which corresponds to a large lattice potential of the form

$$\mathcal{U}(r) = \frac{1}{\epsilon}\left[\cos\left(\frac{r}{\sqrt{\epsilon}}\right) - 1\right] \quad (61)$$

for small ϵ. In this case, we see that even though the solutions are dominated by the large potential more than by the nonlinearity (which is clear when comparing Fig. 17 to Fig. 15), even though they both scale equally. So, even though the amplitude of the wave function is relatively large [of order $O(\epsilon^{-1/2})$], the order $O(\epsilon^{-1})$ potential still dominates. This is in agreement with what we see in some of the solutions of previous sections, such as when the attractive BECs exhibit density that does not tend to a steady state (as radial solutions of the $3+1$ cubic NLS equation with no potential might suggest) due to the influence of the potentials.

In Fig. 18 we consider the large Morse potential $\hat{U}(R) = 2[\exp(-2R) - 2\exp(-R)]$, which takes the form

$$\mathcal{U}(r) = \frac{2}{\epsilon}\left[\exp\left(-\frac{2r}{\sqrt{\epsilon}}\right) - 2\exp\left(-\frac{r}{\sqrt{\epsilon}}\right)\right] \quad (62)$$

for small ϵ. We plot the resulting density curves for the attractive and repulsive BECs and find that there is very little difference between each case. This again demonstrates that the large potentials dominate the dynamics of the BECs in the limit considered.

Physically, the large-potential–large-amplitude approximations obtained here give corrections to the Thomas-Fermi approximation in the sense that the Thomas-Fermi approximation is static (there is no input from kinetic energy). Here we show that in the case of rapidly varying solutions, the kinetic energy term may scale large enough so that it gives an additional contribution. Therefore, for slowly varying solutions the Thomas-Fermi approximation as derived

above is useful, while when the density of the BEC is more rapidly varying in space, we can develop a type of singular perturbation which allows us to adequately address that case as well. In the latter case, we find that the contribution of the potential still dominates the other terms. This is clearly seen in Figs. 17 and 18 in which the strong potential is the primary forcing mechanism for the spatial distribution of the density. In contrast, the nonlinearity and kinetic energy play a far more minor role, as evidenced from the fact that both the attractive and repulsive BECs have quite similar qualitative density distributions. The role of the nonlinear term and the kinetic energy term is then to bring about specific quantitative differences in the density distributions. In the case of the Morse potential, most of the BEC is confined to the central core region. In contrast, the density distribution under the very large lattice potential results in a nonuniform and nearly chaotic appearance. This means that, in the very large potential limit, one may be able to predict the location of density maxima, but one may not be able to predict the relative strength of each maxima. The physical picture is then of a succession of spherical density shells with somewhat highly variable mass concentrations.

C. Solutions with slow space variability

In order to consider solutions that vary slowly with the radial space variable, we consider

$$\Phi(r) = \tilde{\Phi}(\rho), \quad \mathcal{U}(r) = \tilde{U}(\rho), \quad \text{where} \quad \rho = \epsilon r. \tag{63}$$

Then

$$\text{sgn}(g)(\tilde{\Phi} - 2\tilde{\Phi}^3) = \tilde{U}\tilde{\Phi}. \tag{64}$$

We obtain either the zero solution $\tilde{\Phi}(\rho) = 0$ or the nontrivial solution

$$\tilde{\Phi}(\rho) = \sqrt{\frac{1 - \text{sgn}(g)\tilde{U}(\rho)}{2}}, \tag{65}$$

assuming this solution is defined. Note that this is again in the form of a Thomas-Fermi approximation, and this differs from the large-potential–large-amplitude result by a constant. This makes sense, because when either

(i) the solution is slowly varying in the space variable or

(ii) the solution and potential are large, the kinetic energy term $\Phi'' + \frac{2}{r}\Phi'$ is negligibly small relative to the other terms.

Relative to our discussion above regarding the Thomas-Fermi approximation, this result make complete physical sense. In the case of slowly varying density profiles, the kinetic energy is negligible, and hence the remaining terms without derivatives completely determine the spatial profile of the BEC wave function and hence of the density profiles.

D. Very small amplitude limit

In the limit where the amplitude of the wave function is very small (say $\epsilon \ll 1$), yet the potential cannot be considered a small quantity, we approximate (52) by the linear equation

$$\Phi'' + \frac{2}{r}\Phi' + \text{sgn}(g)\Phi = \mathcal{U}(r)\Phi + O(\epsilon^2), \tag{66}$$

where ϵ denotes the amplitude of the wave function. While this equation is linear, it is still nonautonomous and cannot be solved exactly for arbitrary forms of the potential $\mathcal{U}(r)$. Still, we can obtain solutions for specific forms of $\mathcal{U}(r)$.

When the potential is a constant or zero, $\mathcal{U}(r) = \lambda$, we have

$$\Phi(r) = \begin{cases} \epsilon \frac{\sin[\sqrt{\text{sgn}(g)-\lambda}r]}{\sqrt{\text{sgn}(g)-\lambda}r} + O(\epsilon^3) & \text{if} \quad g > 0, \\ \epsilon \frac{\sinh[\sqrt{\text{sgn}(g)-\lambda}r]}{\sqrt{\text{sgn}(g)-\lambda}r} + O(\epsilon^3) & \text{if} \quad g < 0. \end{cases} \tag{67}$$

This is consistent with what we have seen in the density plots of previous sections. In the repulsive case, the radial part of the wave function exhibits damped oscillations with decay in density as $r \to \infty$. Meanwhile, in the attractive case, the nonlinearity tends to focus the solution, and in the absence of this nonlinearity the (relatively large) potential results in growth. Therefore, the higher-order terms help in keeping the solutions bounded in the attractive case.

For the harmonic potential, $\mathcal{U}(r) = \lambda r^2$, we have

$$\Phi(r) = \epsilon \exp\left(-\frac{\sqrt{\lambda}}{2}r^2\right)\text{KM}(r) + O(\epsilon^3), \tag{68}$$

where

$$\text{KM}(r) = \text{KummerM}\left[\frac{3\sqrt{\lambda} - \text{sgn}(g)}{4\sqrt{\lambda}}, \frac{3}{2}, \sqrt{\lambda}r^2\right] \tag{69}$$

and KummerM denotes Kummer's (confluent hypergeometric) M function [37]. In the large r limit, where $\lambda r^2 - \text{sgn}(g) \sim \lambda r^2$, we have the asymptotics

$$\Phi = \begin{cases} \epsilon r^{-1/2}\mathcal{J}_{1/4}\left(\frac{\sqrt{|\lambda|}}{2}r^2\right) + O(\epsilon^3) & \text{if} \quad \lambda < 0, \\ \epsilon r^{-1/2}\mathcal{I}_{1/4}\left(\frac{\sqrt{|\lambda|}}{2}r^2\right) + O(\epsilon^3) & \text{if} \quad \lambda > 0, \end{cases} \tag{70}$$

where $\mathcal{J}_{1/4}$ and $\mathcal{I}_{1/4}$ denote the relevant Bessel functions.

For the Morse potential $\mathcal{U}(r) = \lambda[\exp(-2Ar) - 2\exp(-Ar)]$, we have

$$\Phi(r) = \frac{\epsilon}{r}\exp\left(\frac{A}{2}r\right)\left\{\frac{\text{WW}(0)}{\text{WM}(0)}\text{WM}(r) + \text{WW}(r)\right\} + O(\epsilon^3), \tag{71}$$

where

$$\text{WM}(r) = \text{WhittakerM}\left[\frac{\sqrt{\lambda}}{A}, \frac{\sqrt{-\text{sgn}(g)}}{A}, \frac{2\sqrt{\lambda}}{A}\exp(-Ar)\right], \tag{72}$$

$$\text{WW}(r) = \text{WhittakerW}\left[\frac{\sqrt{\lambda}}{A}, \frac{\sqrt{-\text{sgn}(g)}}{A}, \frac{2\sqrt{\lambda}}{A}\exp(-Ar)\right]. \tag{73}$$

Here WhittakerM and WhittakerW denote the Whittaker M and W functions, respectively [37].

For the lattice potential $\mathcal{U}(r) = \lambda[1 - \cos(r)]$, we have

$$\Phi(r) = \frac{\epsilon}{r}\text{MathieuS}\left\{4[\text{sgn}(g) - \lambda], -2\lambda, \frac{r}{2}\right\} + O(\epsilon^3), \tag{74}$$

where MathieuS denotes the odd Mathieu function with characteristic value $4[\text{sgn}(g) - \lambda]$ and parameter -2λ.

These solutions, obtained for particular exactly solvable cases, can be used to validate some of the perturbation results obtained in earlier sections. In the small amplitude limit, kinetic energy and potential terms dominate, which effectively linearizes the model, allowing for such approximate solutions.

E. Very large mass limit

In the above solutions, we effectively considered cases where the mass m was small or intermediate. If the mass m is very large, then the kinetic energy term vanishes. Furthermore, the transformation (50) will vanish while the potential function (51) will expand. Therefore, in the very large mass limit we should consider Eq. (49) directly without this type of solution assumption. However, while we can no longer consider a solution of the form (50) in the very large mass limit, we shall now show that any solution in the large mass limit must still be a stationary solution.

Taking the limit $m \to \infty$, from Eq. (49) we obtain

$$i\hbar\Psi_t = [V(\mathbf{x}) + g|\Psi|^2]\Psi. \tag{75}$$

Writing $\Phi(\mathbf{x},t) = \mathcal{R}(\mathbf{x},t)\exp(i\Theta(\mathbf{x},t))$, we must have

$$\mathcal{R}_t = 0 \quad \text{and} \quad -\hbar\Theta_t = V(\mathbf{x}) + g\mathcal{R}^2. \tag{76}$$

The former equation implies that $\mathcal{R}$ is constant in time; hence, $\mathcal{R} = \mathcal{R}(\mathbf{x})$. As such, the amplitude is time invariant and the solution is indeed stationary. Then the second equation gives

$$\Theta(\mathbf{x},t) = -\frac{t}{\hbar}[V(\mathbf{x}) + g\mathcal{R}(\mathbf{x})^2]. \tag{77}$$

Hence, in the very large mass limit, the wave function Ψ must take the form of a solution,

$$\Psi(\mathbf{x},t) = \mathcal{R}(\mathbf{x})\exp\left\{-\frac{it}{\hbar}[V(\mathbf{x}) + g\mathcal{R}(\mathbf{x})^2]\right\}. \tag{78}$$

For this limiting case, the amplitude of the wave function is specified through any boundary or initial condition. For instance, $\Psi(\mathbf{x},0) = \mathcal{R}(\mathbf{x})$. In the very large mass limit, the potential only influences the phase of the solution. This is in contrast to the finite mass case, where the phase was space independent (for the type of solution we studied).

Since the choice of $\mathcal{R}(\mathbf{x})$ is arbitrary (it is not determined from the temporal differential equation), it is possible to make a solution of the form (78) stationary. If we pick $\mathcal{R}(\mathbf{x})$ so that $V(\mathbf{x}) + g\mathcal{R}(\mathbf{x})^2 = \Omega$, for some constant Ω, then

$$\mathcal{R}(\mathbf{x}) = \sqrt{\frac{\Omega - V(\mathbf{x})}{g}}. \tag{79}$$

Yet, this is again the Thomas-Fermi approximation, giving a stationary solution

$$\Psi(\mathbf{x},t) = \sqrt{\frac{\Omega - V(\mathbf{x})}{g}}\exp\left[-\frac{i\Omega t}{\hbar}\right]. \tag{80}$$

So, in the very large mass limit, purely stationary solutions do exist and furthermore must take the form of the Thomas-Fermi approximation. Meanwhile, nonstationary solutions [of the more general form (78)] also exist in the marge mass limit, and such solutions contain an arbitrary function which may be specified by any desired boundary conditions.

F. Asymptotic properties of eigenfunctions

Throughout the paper, we have scaled out the central density at $r = 0$, setting it to a constant throughout the plots and the perturbation analysis. We now consider the structural dependence of the solutions on the central density. We show that for acceptable values of the central density, the results obtained up to this point are completely reasonable and capture all interesting qualitative behaviors. For large values of the central density, there can be expansion of the unperturbed solutions, highlighting the nonphysical nature of such cases.

Starting with a radial solution (50) to (49) such that $\Phi(0) = \chi > 0$, we can treat χ as a type of bifurcation parameter. We restrict our attention to eigenfunctions corresponding to the zero potential case, because such functions are what we perturb solutions against in the case of nonzero potentials. Therefore, consider a solution form

$$\Phi(r) = \chi q(r) \tag{81}$$

to (50). Placing this into (49) and neglecting the potential, we obtain the radial equation

$$q''(r) + \frac{2}{r}q'(r) + \mathrm{sgn}(g)[q(r) - 2\chi^2 q(r)^3] = 0. \tag{82}$$

Note that χ enters this equation through the nonlinearity (for a purely linear equation, this multiplicative scaling would not matter). We have the conditions

$$q(0) = 1 \quad \text{and} \quad q'(0) = 0, \tag{83}$$

so that $\Phi(0) = \chi$.

For the repulsive case ($g > 0$), we plot a sample of relevant solutions in Fig. 19. We see that χ does indeed behave like a bifurcation parameter and $\chi = \frac{\sqrt{2}}{2}$ is a critical value. For $0 < \chi < \frac{\sqrt{2}}{2}$, the eigenfunctions corresponding to χ will exhibit oscillatory decay toward zero density for large r. Meanwhile, if $\chi > \frac{\sqrt{2}}{2}$, the eigenfunctions will exhibit unbounded growth, making the solutions nonphysical. If $\chi = \frac{\sqrt{2}}{2}$, the eigenfunction is constant and hence degenerate. These are all possible solutions parameterized in χ, and we see that the physical solutions correspond to $0 < \chi < \frac{\sqrt{2}}{2}$. Therefore, it makes sense to consider perturbations of the decaying eigenfunctions when studying the equations which include potential.

To understand why the eigenfunctions which decay must oscillate in the repulsive case, as opposed to, say, decaying monotonically, note that as the eigenfunctions decay, they enter the small amplitude regime. As such, for large enough r, we must have $|q(r)|^3 \ll |q(r)|$, so the linear term dominates. This means that (82) can be replaced with

$$q''(r) + \frac{2}{r}q'(r) + q(r) = 0 \tag{84}$$

for large r. Therefore, in the repulsive case, the eigenfunctions should obey

$$q(r) = \frac{q_1\cos(r) + q_2\sin(r)}{r} \tag{85}$$

for real constants q_1 and q_2 as $r \to \infty$ whenever the eigenvalue χ satisfies $0 < \chi < \frac{\sqrt{2}}{2}$.

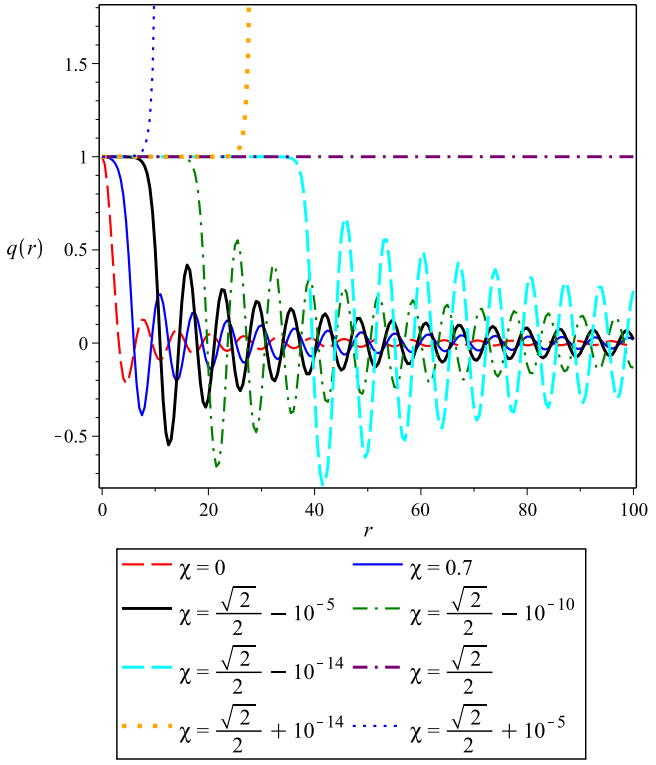

FIG. 19. (Color online) Plot of the scaled radial eigenfunctions $q(r)$ for the repulsive BEC when the central density is $\Phi(0) = \chi$, i.e., $\Phi(r) = \chi q(r)$, $q(0) = 1$. We see that $\chi = \frac{\sqrt{2}}{2}$ is a critical value. For $0 < \chi < \frac{\sqrt{2}}{2}$, the eigenfunctions will exhibit oscillatory decay toward zero density for large r. Meanwhile, if $\chi > \frac{\sqrt{2}}{2}$, the eigenfunctions will exhibit unbounded growth, making the solutions nonphysical. If $\chi = \frac{\sqrt{2}}{2}$, the eigenfunction is degenerate (in particular, a constant), which corresponds to a steady state in the space variable. Therefore, it makes sense to expand our perturbation solutions about the eigenfunctions which exhibit decay, and this is exactly what we have done in earlier sections.

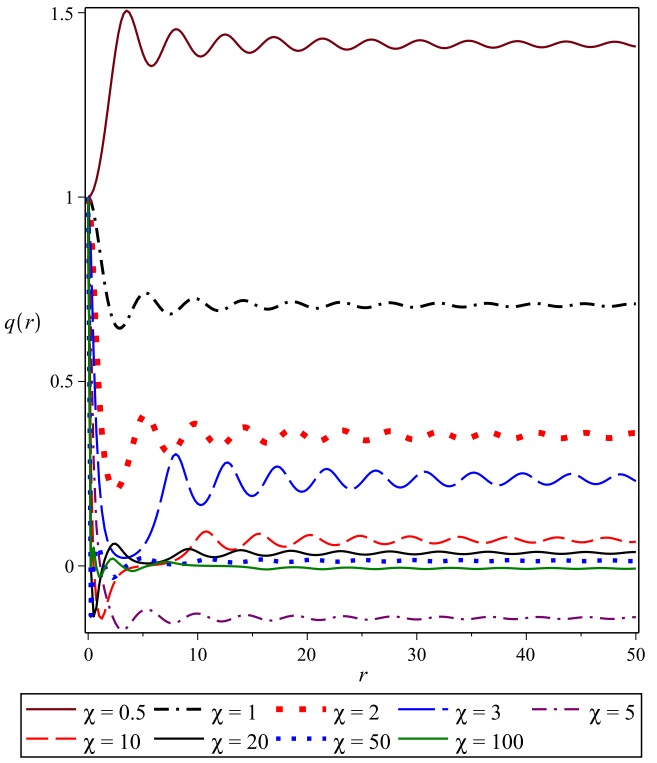

FIG. 20. (Color online) Plot of the scaled radial eigenfunctions $q(r)$ for the attractive BEC when the central density is $\Phi(0) = \chi$, i.e., $\Phi(r) = \chi q(r)$, $q(0) = 1$. Solutions tend to either of the $\pm\frac{1}{\sqrt{2}\chi}$ spatial fixed points, and since the linear terms dominate (as we have shown in the above analysis) the solutions will exhibit damped oscillations as they tend toward these values.

For the attractive case, the zero equilibrium is unstable, and the decaying solutions will be drawn toward one of the nonzero spatial equilibria to Eq. (82), which are easily seen to be $\pm\frac{1}{\sqrt{2}\chi}$. Since the solutions tend asymptotically toward one of these nonzero values, it might be tempting to think that nonlinear effects will dominate in the large r limit. However, note that the solutions should behave like

$$q(r) = \pm\frac{1}{\sqrt{2}\chi} + Q(r) \tag{86}$$

for some function $Q(r)$ satisfying $Q(r) \to 0$ as $r \to \infty$. Placing (86) into (82) and noting $g < 0$ for the attractive case, we arrive at

$$Q''(r) + \frac{2}{r}Q'(r) - \left[\pm\frac{1}{\sqrt{2}\chi} + Q(r)\right] \times\left\{1 - 2\chi^2\left[\pm\frac{1}{\sqrt{2}\chi} + Q(r)\right]^2\right\} = 0. \tag{87}$$

In the large r limit, $|Q(r)|^3 \ll |Q(r)|^2 \ll |Q(r)|$, and keeping only linear terms, we obtain

$$Q''(r) + \frac{2}{r}Q'(r) + 2Q(r) = 0. \tag{88}$$

We therefore find that

$$Q(r) = \frac{q_1\cos(\sqrt{2}r) + q_2\sin(\sqrt{2}r)}{r}, \tag{89}$$

for real constants q_1 and q_2 as $r \to \infty$. Therefore, when r is sufficiently large, we must have

$$q(r) = \pm\frac{1}{\sqrt{2}\chi} + \frac{q_1\cos(\sqrt{2}r) + q_2\sin(\sqrt{2}r)}{r} \tag{90}$$

for the attractive case. Hence, the eigenfunctions for the attractive case also exhibit oscillations as they decay, and as such there are no monotone decreasing eigenfunctions which remain bounded.

In Fig. 20 we plot sample numerical solutions to (82) for various values of χ, and the exact numerical solutions demonstrate the behavior predicted in the large-r asymptotics derived above. Therefore, the solutions tend toward one of two spatial fixed points. By the above analysis, and what we see from the numerics, the solutions will always exhibit damped oscillations as they tend toward these asymptotic values, since the solutions are asymptotically within the linear regime for

the large-r limit. Since the unperturbed solutions behave in this matter, it makes sense to perturb these solutions in the presence of small potentials. Note that if the potential exerts a strong enough influence on the solutions, it may effectively switch the solution from attractive to repulsive, resulting in solutions which decay toward zero in density even if the governing cubic NLS equation is in the attractive regime. We observe this behavior in some of the perturbation and numerical solutions of Sec. VI.

VIII. DISCUSSION

A. Summary

Throughout this paper, we have been able to study solutions both analytically (through a perturbation approach) and numerically for both attractive and repulsive BECs under the $3+1$ cubic NLS equation with arbitrary forms of the confining potential. The stationary solutions studied here correspond to radially symmetric BECs in three spatial dimensions. Such results generalize the 1D and 2D results considered by the authors previously [22–24]. Numerical solutions have also been discussed in a number of cases where the potential was permitted to be larger, and in the attractive case in the degenerate limit $\epsilon \to 0$.

For the repulsive BECs, there are essentially two physical scenarios that emerge. First, the BEC may be confined to a small region surrounding the origin. Such BECs are appropriately confined by the trap and may be observed experimentally near the origin in high concentrations. Second, one may have a local density maxima at the origin, with auxiliary density maxima occurring at positive values of the radius. In this case, BECs can be found at density maxima shells that surround and gradually radiate out from the origin. In each of these shells, the density is locally large, whereas in regions between these shells there is a drop in observed density of the BEC. These shells are spherical in form, owing to the radial symmetry of the potential traps in 3D.

Regarding the attractive BECs, the strength of the potentials will strongly influence the behavior of the BEC wave functions. First, in the case where the potential is radially unbounded, the solutions behaved like those found in the repulsive case, with either a single spherical density region or the density allocated along a number of shells surrounding the origin. Meanwhile, when the confining potential is relatively small, we can observe positive-density BECs even as the radius becomes large. The wave function then gives a cloud of BECs which is radially unbounded. This means that these types of solutions exist with a nonzero background concentration of the BEC. However, this large BEC cloud can still have global and local density maxima, in which a much larger density of the BEC can be found.

We finally obtained some numerical and qualitative results for the case when the amplitude of the wave function and the size of the potential are in the nonperturbative regime. In particular, we considered cases where the potential is small but the amplitude is not small, the potential and the amplitude are large, the kinetic energy term is small, the amplitude is small, but the potential is not small. We also considered the very large mass limit. In cases where the potential is large, the potential dominates the form of the wave function, akin to the Thomas-Fermi limit. Similarly, when the kinetic energy term is small, or the mass is very large, we recover solutions that agree with the Thomas-Fermi limit.

B. Size of the potential and the wave functions

In the so-called perturbative limit, where both the potential and the amplitude of the wave function for the BEC are small enough, perturbation and numerical solutions have been used at various points to generate the plots provided in Secs. IV and VI. The specific values of ϵ for which perturbation solutions may be used will vary from model to model. We often find that $\epsilon = O(10^{-1})$ or smaller gives accurate perturbation solutions for the repulsive case. The attractive case is a bit more complicated. The attractive BECs which tend toward a zero density as the radius increases from the origin can be accurately described by the perturbation results when $\epsilon = O(10^{-1})$ or smaller. Unfortunately, those attractive BECs which asymptotically approach some positive density fail to be accurately approximated by the perturbation approach. The reason for this is that the asymptotic density scales like $|\phi(r)|^2 \sim \epsilon^{-1}$ as $r \to \infty$, and hence the small ϵ regime is actually a singular limit, rendering the perturbation results useless for these particular BECs. Interestingly, the large ϵ limit is well defined for such BECs, although the perturbation results (relying on small ϵ) still are not useful. So those attractive BECs with asymptotic behavior $|\phi(r)|^2 \sim \epsilon^{-1}$ as $r \to \infty$ must be numerically simulated.

In the case where the potential is large ($\epsilon \gg 1$), one can obtain a perturbation expansion in inverse powers of ϵ. At lowest order, such an expansion will agree directly with the Thomas-Fermi approximation (provided kinetic energy is small enough). Similarly, if kinetic energy is small, or if mass is very large, then the solutions are in agreement with the Thomas-Fermi approximation. There is an interesting limit in which the solutions are rapidly varying in space and the confining potential is large. In such a limit, we can obtain rapidly varying solutions with large kinetic energy, even in the presence of the large potential. Such solutions themselves are large, but are of orders of magnitude smaller than the large potential. Such a case can be seen as a perturbation to the Thomas-Fermi approximation. In the limit where the amplitude is very small, but the potential and kinetic energy terms are not small (in a relative sense), then the model is effectively linearized and one can obtain closed-form solutions under specific potentials.

C. Physical implications from potentials of various sizes

In considering small and intermediate potentials and wave functions, we observed two general trends concerning potentials: Certain potentials were highly effective at concentrating most of the mass of the BEC near the origin in a core spherical region. Other potentials were far less effective, leading to larger secondary density maxima (which take the form of concentric density shells surrounding the primary core density region at the origin. The strongest potentials were able to adequately confine both attractive and repulsive BECs. On the other hand, weaker potentials were more effective when containing the repulsive BECs, as the tails of their respective wave functions decay for larger values of the radial coordinate. On the other

hand, such weaker potentials were not so effective at containing the attractive BECs, and in such cases the attractive BECs behaved much like the uncontained solutions found in the $3+1$ cubic NLS equation with zero potential. Since attractive BECs naturally tend to some positive ambient density under the $3+1$ cubic NLS model, this means that a potential is necessary in order to force the greatest density concentration into any specific region. In contrast, the repulsive BECs can be found in a spherical centralized mass around the origin.

For all cases considered, when there is a primary core region of BEC density at the origin, there are secondary density maxima that occur in density shells that surround the core region. These secondary density maxima exist whenever there is a repulsive BEC or whenever the attractive BEC is forced by a potential into occupying the region near the origin. The existence of these maxima is inherited from the $3+1$ cubic NLS equation, as was seen when we considered the zero-potential limit. Oscillating tails in the wave function are fundamental to the radially symmetric solutions in three spatial dimensions. This is in contrast to the case of one spatial dimension, in which solitons can be obtained (owing to the integrability of the 1D model). While one cannot completely remove these secondary density maxima, as we show in Secs. IV and VI, one can pick specific forms of the confining potentials in order to minimize the mass in these secondary density shells, in order to ensure that nearly all of the mass lies in the central spherical region. Therefore, the specific choice of potential can matter a great deal, as is known in experiment design for studying BECs.

Lattice potentials which have many local potential wells can be shown to allow one to control the secondary density shells inherent under the model studied. In cases where the appearance of density maxima away from the core region cannot be helped, these potentials allow one to control the location of these secondary density maxima. In effect, they allow one to predict exactly where any secondary density shells of BEC concentration will be located away from the central spherical region. In contrast, for other types of potentials, the appearances of these secondary density maxima can vary quite a bit with the model parameter, as their location can be influenced by the nonlinearity of the problem. This is another way in which choosing the right potential can be beneficial in experimentally observing the BEC concentrations in 3D.

In the case where the potential is made large, these secondary density maxima can be reduced further in magnitude, and in the very large potential limit where the potential dominates the other terms in the cubic NLS equation the results reduce to the Thomas-Fermi approximation. Additionally, when the kinetic energy term is small or the mass is very large, the results can be shown to reduce to the Thomas-Fermi limit. Meanwhile, if the amplitude of the wave function is very small, relative to the kinetic energy and the potential, the governing equation is effectively linearized, and for many potentials the model becomes exactly solvable. The qualitative results for this case are in agreement with the earlier perturbative results obtained in the small ϵ limit.

There also exist rapidly varying solutions in space, under the large potential limit. Such solutions can be seen as a next order correction to the Thomas-Fermi approximation, in which the kinetic energy term is maintained due to the rapid space variations. Still, such solutions scale as the square root of the potential; hence, such results are essentially corrections to that limit. As we saw in Sec. VII, the rapidly varying solutions are strongly determined by the choice of potential used, much more so than whether such solutions are attractive or repulsive. Physically, this again highlights the importance of selecting an appropriate potential.

D. Conclusions

We have determined qualitative behaviors of both attractive and repulsive BECs in three spatial dimensions, assuming radial symmetry of solutions. This radial symmetry yields BECs which can occur either (i) in a spherical region surrounding the origin, (ii) in spherical density shells surrounding the origin, or (iii) in an infinite cloud with local density minima and maxima occurring radially. The repulsive BECs correspond to cases (i) and (ii), whereas the attractive BECs correspond to cases (i), (ii), and (iii), depending on the strength and form of the potential. There are qualitative differences in the solutions as one transitions from fairly weak confining potentials to strong confining potentials. In the limit where the potentials are particularly large, they dominate the behavior of the wave functions, akin to what one sees in the Thomas-Fermi limit. For more intermediate or small potentials, the kinetic energy term and nonlinearity also play a role in the structure of the solutions.

Without the radial symmetry, one could still solve (1), but in this instance it would be necessary to simulate the governing partial differential equation directly, subject to any initial or boundary conditions. One could also seek self-similar solutions to (1) (as opposed to radially symmetric solutions); however, one would need to consider very special potential traps in order to study the solutions. Such solutions are typically only sought in the case where the potential is removed (so that one simply considers the cubic NLS equation without potential), as there would likely need to be very specific time dependence in the potential in order for a self-similar wave function solution to exist. Analytical results could be possible for some very specific nonradial potentials, but we would not expect many general results in the absence of some symmetries. Results might also be obtained for time-dependent potentials, which can be switched on and strengthened over an interval of time, but again we would not expect general results with likely only very special cases being solvable.

Alternately, one could consider BECs on other spatial structures, such as manifolds. This type of work has been considered for the linear Schrödinger equation under various potentials [38], but not for BECs governed by NLS equations. For instance, one could consider BECs on 2D surfaces embedded within 3D space. These BECs would be more challenging to work with than simple BECs in 2D space, such as the radial solutions of [24]. Such work would be most relevant for BECs on nonflat surfaces. In particular, it would be interesting to study the structure of BECs on curved or hyperbolic surfaces, as perhaps one can pick specific surfaces to enhance persistence or stability of the BECs.

Studying stability of oscillating solutions can prove more complicated than studying solutions of more well behaved solutions, such as solitons. In the soliton case, once can

apply the Vakhitov and Kolokolov criteria to study the solutions [39]. Spectral approaches in this vein can be used to study oscillating or nonstationary solutions, although this is often more complicated than in the soliton case [40]. For the $3+1$ model, one would need to contend with the oscillation solutions and with a nonautonomous equation in the space variable (due to the potential term), which would complicate any such analysis. It may still be possible to perform some type of stability analysis numerically or under some approximations, for the types of solutions we obtain in this paper, and such a study may be of interest in future work for the 3D BECs.

ACKNOWLEDGMENT

K. Mallory supported in part by the NSF Graduate Research Fellowship under Grant No. DGE-1058262.

[1] F. Dalfovo, S. Giorgini, L. P. Pitaevskii, and S. Stringari, Rev. Mod. Phys. **71**, 463 (1999); L. D. Carr, M. A. Leung, and W. P. Reinhardt, J. Phys. B: At. Mol. Opt. Phys. **33**, 3983 (2000); M. Key, I. G. Hughes, W. Rooijakkers, B. E. Sauer, E. A. Hinds, D. J. Richardson, and P. G. Kazansky, Phys. Rev. Lett. **84**, 1371 (2000); N. H. Dekker, C. S. Lee, V. Lorent, J. H. Thywissen, S. P. Smith, M. Drndic, R. M. Westervelt, and M. Prentiss, *ibid.* **84**, 1124 (2000).

[2] M. Kunze *et al.*, Phys. D (Amsterdam, Neth.) **128**, 273 (1999); Y. S. Kivshar, T. J. Alexander, and S. K. Turitsyn, Phys. Lett. A **278**, 225 (2001).

[3] S. Theodorakis and E. Leontidis, J. Phys. A **30**, 4835 (1997); F. Barra, P. Gaspard, and S. Rica, Phys. Rev. E **61**, 5852 (2000).

[4] J. C. Bronski, L. D. Carr, B. Deconinck, and J. N. Kutz, Phys. Rev. Lett. **86**, 1402 (2001).

[5] B. P. Anderson and M. A. Kasevich, Science **282**, 1686 (1998); E. W. Hagley *et al.*, *ibid.* **283**, 1706 (1999).

[6] Y. B. Ovchinnikov, J. H. Muller, M. R. Doery, E. J. D. Vredenbregt, K. Helmerson, S. L. Rolston, and W. D. Phillips, Phys. Rev. Lett. **83**, 284 (1999).

[7] D. Jaksch, C. Bruder, J. I. Cirac, C. W. Gardiner, and P. Zoller, Phys. Rev. Lett. **81**, 3108 (1998); G. K. Brennen, C. M. Caves, P. S. Jessen, and I. H. Deutsch, *ibid.* **82**, 1060 (1999).

[8] D.-I. Choi and Q. Niu, Phys. Rev. Lett. **82**, 2022 (1999).

[9] L. D. Carr, C. W. Clark, and W. P. Reinhardt, Phys. Rev. A **62**, 063610 (2000).

[10] L. D. Carr, C. W. Clark, and W. P. Reinhardt, Phys. Rev. A **62**, 063611 (2000).

[11] X.-F. Zhou, S.-L. Zhang, Z.-W. Zhou, B. A. Malomed, and H. Pu, Phys. Rev. A **85**, 023603 (2012).

[12] H. Cartarius and G. Wunner, Phys. Rev. A **86**, 013612 (2012).

[13] R. D'Agosta and C. Presilla, Phys. Rev. A **65**, 043609 (2002).

[14] F. Schreck, L. Khaykovich, K. L. Corwin, G. Ferrari, T. Bourdel, J. Cubizolles, and C. Salomon, Phys. Rev. Lett. **87**, 080403 (2001).

[15] M. H. Anderson, J. R. Ensher, M. R. Matthew, C. E. Wieman, and E. A. Cornell, Science **269**, 198 (1995).

[16] M.-O. Mewes, M. R. Andrews, N. J. van Druten, D. M. Kurn, D. S. Durfee, and W. Ketterle, Phys. Rev. Lett. **77**, 416 (1996).

[17] J. R. Abo-Shaeer, C. Raman, J. M. Vogels, and W. Ketterle, Science **292**, 476 (2001).

[18] A. L. Fetter, Phys. Rev. A **64**, 063608 (2001).

[19] I. Coddington, P. Engels, V. Schweikhard, and E. A. Cornell, Phys. Rev. Lett. **91**, 100402 (2003); A. L. Fetter, B. Jackson, and S. Stringari, Phys. Rev. A **71**, 013605 (2005); D. L. Feder and C. W. Clark, Phys. Rev. Lett. **87**, 190401 (2001); U. R. Fischer and G. Baym, *ibid.* **90**, 140402 (2003).

[20] C. M. Savage, N. P. Robins, and J. J. Hope, Phys. Rev. A **67**, 014304 (2003).

[21] L. J. Garay, J. R. Anglin, J. I. Cirac, and P. Zoller, Phys. Rev. Lett. **85**, 4643 (2000); Phys. Rev. A **63**, 023611 (2001).

[22] K. Mallory and R. A. Van Gorder, Phys. Rev. E **88**, 013205 (2013).

[23] K. Mallory and R. A. Van Gorder, Phys. Rev. E **89**, 013204 (2014).

[24] K. Mallory and R. A. Van Gorder, Phys. Rev. E **90**, 023201 (2014).

[25] E. M. Lifshitz and L. P. Pitaevskii, *Statistical Physics Part 2: Landau and Lifshitz Course of Theoretical Physics* (Butterworth-Heinemann, Oxford, UK, 1980).

[26] Z. X. Liang, Z. D. Zhang, and W. M. Liu, Phys. Rev. Lett. **94**, 050402 (2005); S. K. Adhikari, Phys. Rev. E **62**, 2937 (2000); V. M. Pérez-García, H. Michinel, J. I. Cirac, M. Lewenstein, and P. Zoller, Phys. Rev. A **56**, 1424 (1997); W. Bao, D. Jaksch, and P. A. Markowich, J. Comput. Phys. **187**, 318 (2003).

[27] G. Theocharis, Z. Rapti, P. G. Kevrekidis, D. J. Frantzeskakis, and V. V. Konotop, Phys. Rev. A **67**, 063610 (2003).

[28] M. Landtman, Phys. Lett. A **175**, 147 (1993).

[29] P. M. Morse, Phys. Rev. **34**, 57 (1929).

[30] Y. Zhou, M. Karplus, K. D. Ball, and R. S. Bery, J. Chem. Phys. **116**, 2323 (2002).

[31] W. C. Stwalley and L. H. Nosanow, Phys. Rev. Lett. **36**, 910 (1976); B. D. Esry and C. H. Greene, Phys. Rev. A **60**, 1451 (1999).

[32] S. Burger, F. S. Cataliotti, C. Fort, F. Minardi, M. Inguscio, M. L. Chiofalo, and M. P. Tosi, Phys. Rev. Lett. **86**, 4447 (2001); M. Greiner, I. Bloch, O. Mandel, T. W. Hänsch, and T. Esslinger, *ibid.* **87**, 160405 (2001); M. Greiner, O. Mandel, T. W. Hänsch, and I. Bloch, Nature (London) **419**, 51 (2002); C. Orzel, A. K. Tuchman, M. L. Fenselau, M. Yasuda, and M. A. Kasevich, Science **291**, 2386 (2001); G. Chong, W. Hai, and Q. Xie, Phys. Rev. E **70**, 036213 (2004).

[33] G. J. Milburn, J. Corney, E. M. Wright, and D. F. Walls, Phys. Rev. A **55**, 4318 (1997); Y. Shin, M. Saba, T. A. Pasquini, W. Ketterle, D. E. Pritchard, and A. E. Leanhardt, Phys. Rev. Lett. **92**, 050405 (2004); A. Smerzi, S. Fantoni, S. Giovanazzi, and S. R. Shenoy, *ibid.* **79**, 4950 (1997); L. Pitaevskii and S. Stringari, *ibid.* **87**, 180402 (2001); J. Ruostekoski and D. F. Walls, Phys. Rev. A **58**, R50 (1998); R. W. Spekkens and J. E. Sipe, *ibid.* **59**, 3868 (1999); K. W. Mahmud, H. Perry, and W. P. Reinhardt, *ibid.* **71**, 023615 (2005).

[34] G. Roati *et al.*, Nature (London) **453**, 895 (2008); F. S. Cataliotti, L. Fallani, F. Ferlaino, C. Fort, P. Maddaloni, and M. Inguscio, New J. Phys. **5**, 71 (2003); A. Smerzi and A. Trombettoni, Phys. Rev. A **68**, 023613 (2003); K. J. H. Law, P. G. Kevrekidis,

B. P. Anderson, R. Carretero-González, and D. J. Frantzeskakis, J. Phys. B: At. Mol. Opt. Phys. **41**, 195303 (2008).

[35] L. Fallani, L. De Sarlo, J. E. Lye, M. Modugno, R. Saers, C. Fort, and M. Inguscio, Phys. Rev. Lett. **93**, 140406 (2004).

[36] J. Brand and A. R. Kolovsky, Eur. Phys. J. D **41**, 331 (2007).

[37] M. Abramowitz and I. Stegun, eds., *Handbook of Mathematical Functions* (Dover, New York, 1972).

[38] R. A. Van Gorder, J. Math. Phys. **51**, 122104 (2010); J. Math. Chem. **50**, 1420 (2012).

[39] M. G. Vakhitov and A. A. Kolokolov, Sov. Radiophys. **16**, 783 (1973); V. G. Makhankov, Y. P. Rybakov, and V. I. Sanyuk, Phys.-Usp. **37**, 113 (1994); D. V. Skryabin and W. J. Firth, Phys. Rev. E **58**, R1252 (1998); P. B. Lundquist, D. R. Andersen, and Yu. S. Kivshar, *ibid.* **57**, 3551 (1998); D. Mihalache, D. Mazilu, and L. Torner, Phys. Rev. Lett. **81**, 4353 (1998); B. A. Malomed, D. J. Kaup, and R. A. Van Gorder, Phys. Rev. E **85**, 026604 (2012).

[40] R. A. Van Gorder, J. Phys. Soc. Jpn. **82**, 064005 (2013); **82**, 094005 (2013); **83**, 054005 (2014).